Variability of North Atlantic CO_2 fluxes for the 2000–2017 period estimated from atmospheric inverse analyses

Zhaohui Chen[1], Parvadha Suntharalingam[1], Andrew J. Watson[2], Ute Schuster[2], Jiang Zhu[3], and Ning Zeng[4]

[1]School of Environmental Sciences, University of East Anglia, Norwich, NR4 7TJ, UK.
[2]College of Life and Environmental Sciences, University of Exeter, Exeter, EX4 4RJ, UK.
[3]International Center for Climate and Environment Sciences, Institute of Atmospheric Physics, Chinese Academy of Science, Beijing,10029, China.
[4]Department of Atmospheric and Oceanic Science, and Earth System Science Interdisciplinary Center, University of Maryland, College Park, Maryland, 20742, USA

Correspondence to: Zhaohui Chen (Zhaohui.chen@uea.ac.uk)

Abstract. We present new estimates of the regional North Atlantic (15°N–80°N) CO_2 flux for the 2000–2017 period using atmospheric CO_2 measurements from the NOAA long term surface site network in combination with an atmospheric carbon cycle data assimilation system (GEOSChem–LETKF). We ~~also~~ assess the sensitivity of flux estimates to alternative ocean CO_2 ~~the representation of the~~ prior ~~ocean~~ flux distribution and to the ~~associated~~ specification of ~~prior flux~~ uncertainti~~es~~ associated with ocean fluxes., ~~including a specification that is dependent on the agreement among the multiple representations of the prior ocean flux.~~ We present a new scheme to characterize uncertainty in ocean prior fluxes, derived from a set of eight surface pCO_2–based ocean flux products, which reflects uncertainties associated with measurement density and pCO_2–interpolation methods. This scheme provides improved model performance, in comparison to fixed prior uncertainty schemes, based on metrics of model–observation differences at the network of surface sites. Long term average posterior flux estimates for the 2000–2017 period from our GEOSChem–LETKF analyses are -0.~~26~~255±0.~~04~~ 037 PgC y^{-1} for the subtropical basin (15°N–50°N), and -0.~~25~~203±0.~~04~~ 037 PgC y^{-1} for the subpolar region (50°N–80°N, eastern boundary at 20°E). Our basin–scale estimates of ~~the amplitude of~~ interannual variability (IAV) are 0.~~037~~036±0.006 PgC y^{-1} and 0.~~025~~034±0.009 PgC y^{-1} for subtropical and subpolar regions respectively. We find ~~a~~ statistically significant trend in carbon uptake for the subtropical and subpolar North Atlantic of -0.~~062~~064±0.~~009~~ 007 and -0.063±0.008 PgC y^{-1} $decade^{-1}$ ~~;over this period.~~ these trends are of comparable magnitude to estimates from surface ocean pCO_2–based flux products, but larger, by a factor of 3-4, than trends estimated from global ocean biogeochemistry models.

1 Introduction

The ocean plays a key role in the global carbon budget, accounting for 2.5±0.6 PgC y^{-1} ~~(approximately 26%)~~ of net CO_2 ~~the~~ uptake from the atmosphere ~~of global fossil emissions~~ during the last decade (period 2009-201~~8~~), a level equivalent to ~26% of global fossil CO_2 emissions (Friedlingstein et al., 2019). The North Atlantic ocean has been identified a region of significant

net oceanic CO_2 uptake in a range of recent analyses (Schuster et al., 2013, Landschützer et al., 2013, Lebehot et al., 2019), and also the location of the largest Northern Hemisphere uptake of anthropogenic CO_2 in recent decades (Gruber et al., 2019, Khatiwala et al., 2013, Sabine et al., 2004). Recent estimates of net air–sea CO_2 fluxes derived from sea surface partial pressure CO_2 measurements (pCO_2) indicate net annual uptake for the North Atlantic ~~of -0.47 ±0.08 PgC y^{-1}~~ over~~for~~ the past decade (20~~19~~90~~9~~–2018)~~09~~ with a range of 0.35–0.55 PgC y^{-1} ~~period~~ (Landschutzer et al., 2016; Rodenbeck et al., 2013; Zeng et al., 2015; Watson et al., 2020~~Schuster et al., 2013, equivalent to about 20% of global ocean CO_2 uptake~~), and equivalent to about 14%–22% of the global net ocean carbon ocean sink reported for this period.~~.~~

Regionally aggregated air–sea CO_2 fluxes over the North Atlantic basin also display significant variability on interannual (Watson et al., 2009) and decadal timescales (Landschützer et al., 2016, 2019). Based on analyses of surface pCO_2 measurements, variations in regional pCO_2 trends were observed in the subtropical and subpolar regions, potentially associated with large-scale climate oscillations such as the North Atlantic Oscillation and the Atlantic Multi-decadal Variation (McKinley et al., 2011, Landschützer et al., 2019, Macovei et al., 2020). Devries et al. (2019) estimated a negative trend (i.e., a strengthening ocean sink) in North Atlantic CO_2 uptake ~~based on analysis of pCO_2 based estimates and ocean models~~ for the 2000–2009 period based on analysis of pCO_2-based estimates and ocean models. ~~In addition,~~ Lebehot et al. (2019) f~~ou~~nd statistically significant ~~distinct differences between~~ trends in surface ocean CO_2 fugacity (fCO_2) for the 1992–2014 period ~~derived~~ from both observation-based surface mapping methods and ~~those~~ from the CMIP5 Earth System models.

R~~These r~~ecent analyses of North Atlantic air–sea CO_2 fluxes have primarily been based on 'bottom-up' methods of varying complexity which use interpolated surface ocean pCO_2 distributions (derived from in -situ pCO_2 measurements) in combination with parameterizations of air–sea gas exchange (e.g., Landschützer et al., 2013; Rödenbeck et al., 2015; Takahashi et al., 2002, ~~; Takahashi et al.,~~ 2009). Estimates of air–sea CO_2 fluxes have also been derived by alternative methods such as global ocean biogeochemical models (e.g., Buitenhuis et al.,2013; Law et al., 2017), and 'top-down' methods which involve the application of inverse analyses or data assimilation methods to atmospheric and oceanic CO_2 measurements (e.g., Gruber et al., 2009, Mikaloff-Fletcher et al., 2006, Gurney et al., 2003, Peylin et al., 2013). 'Top-down' analyses estimate surface CO_2 fluxes by using information on observed gradients in atmospheric CO_2 together with atmospheric transport constraints (typically from 3 D atmospheric models) and prior information on the magnitude and associated uncertainties of surface CO_2 flux distributions (Rödenbeck et al., 2003; van der Laan–Luijkx et al., 2017; Peters et al., 2005; Peylin et al., 2013; Chevallier et al., 2014; Gaubert et al., 2019).

~~Atmospheric CO_2 inversions estimate surface CO_2 fluxes by using information on observed gradients in atmospheric CO_2 together with atmospheric transport constraints (typically from 3 D atmospheric models) and prior information on surface CO_2 flux distributions (Rödenbeck et al., 2003; van der Laan–Luijkx et al., 2017; Peters et al., 2005; Peylin et al., 2013; Chevallier et al., 2014; Gaubert et al., 2019). Previous studies have noted some discrepancies between estimates of regional ocean fluxes from the different methods. For example, Peylin et al. (2013) noted the limited constraints provided by atmospheric CO_2 measurements on land–ocean carbon flux partitioning for some regions, and noted the potential for "flux leakage" between land and ocean flux estimates (e.g., the northern ocean fluxes).~~ Previous studies also ~~found~~ note that estimates of carbon fluxes

from the atmospheric inverse method are sensitive to the specification of the prior flux distribution and its associated uncertainty distribution (Carouge et al., 2010; Chatterjee et al., 2013; Peylin et al., 2013); While there have been recent studies evaluating the sensitivity of land−based carbon flux estimates to specification of the prior flux and its uncertainty, there ~~the variation of regional ocean fluxes~~ has been far less examination of ocean flux estimates~~ed~~ from~~by previous~~ inverse studies. Several global inverse model assessments of the past decade have

~~Previous inverse estimates of ocean CO_2 fluxes have predominantly~~ relied on the climatological ocean~~ to~~ atmosphere CO_2 flux ~~distribution~~ database of Takahashi et al. (2009) to specify prior ocean fluxes. In view of the limited information available on the temporal and spatial variability of ocean carbon fluxes from this climatological ocean database, these inverse analyses have adopted different approaches to the specification of prior uncertainty for ocean fluxes, ranging from uncertainties derived from a separate ocean model inversion (in the case of Nassar et al., 2011), to a specified percentage of the prior flux magnitude (Feng et al., 2016, Liu et al., 2016).~~for use as the a priori flux estimate (e.g., Nassar et al., 2011; Feng et al., 2009, 2016; Deng et al., 2016). These analyses often use different methods to specify the level of flux uncertainty assigned to the ocean prior fluxes. For example, the inverse analyses of Feng et al. (2016) and Deng et al. (2016) use prior flux uncertainty levels of 0.6 PgC y^{-1} (equivalent to 44% of the ocean flux total) , i.e., a level of uncertainty twice as large as the uncertainty in Nassar et al. (2011).~~

~~Here~~ In this study we present a new long term estimate of North Atlantic air−sea CO_2 fluxes for recent decades (period 2000−2017) using atmospheric inverse methods. We focus in particular on the specification of prior ocean fluxes (including sensitivity of flux estimates to alternative prior flux distributions) and on their associated flux uncertainties. To our knowledge these influences on inverse estimates of North Atlantic CO_2 flux have not been assessed previously. We use the carbon cycle data assimilation system GEOSChem−LETKF (GCL, described further in Sect. 2) which combines the global atmospheric CO_2 transport model GEOS−Chem (Nassar et al., 2010) with the Localized Ensemble Transform Kalman Filter (LETKF) data assimilation system (Hunt et al., 2007; Miyoshi et al., 2007; Liu et al., 2019). In recent years several new global air–sea CO_2 flux products have been developed based on mappings of ocean surface pCO_2 measurements (e.g., Landschutzer et al., 2016, Rodenbeck et al., 2014, Watson et al., 2020, and products reported in the intercomparison of Roedenbeck et al., 2015). These ocean flux distributions are frequently derived from interpolations of surface ocean pCO_2 measurements from the SOCAT database (Bakker et al., 2016) together with parameterizations of air–sea gas exchange. Following recent updates, the surface ocean pCO_2 database SOCATv2020 (https://www.socat.info/index.php/data-access/), now includes over 28 million surface ocean carbon measurements. The SOCAT database provides a valuable resource towards the development of bottom–up estimates of ocean–atmosphere CO_2 fluxes, and a compilation of these flux products is reported in the recent Global Carbon Budget (Friedlingstein et al., 2020). The increased range of global air–sea CO_2 flux products available (beyond the Takahashi et al., 2009 climatology) provides a valuable opportunity to develop an improved representation of air–sea CO_2 flux variability and a more robust characterization of the uncertainties associated with ocean carbon fluxes. In this study we employ some of the recently developed ocean CO_2 flux products to provide a new method of characterizing the prior ocean flux uncertainty used for atmospheric inverse analyses. The methodology is based on the ensemble spread of the multiple ocean flux products,

and reflects underlying uncertainties in these products, such as those associated with sampling density of the surface measurements and interpolation method employed. It provides a spatially and temporally variable specification of prior flux uncertainty that will be of value to the inverse modeling community. ~~An additional focus of our analysis is to evaluate the sensitivity of flux estimates to alternative a priori flux distributions and uncertainty specifications for oceanic CO_2 fluxes. To our knowledge these influences on North Atlantic flux estimates have not been assessed previously.~~

The remainder of the paper is organized as follows: Section 2 covers the methodology of the atmospheric inverse analysis, outlining the carbon cycle data assimilation system (GEOSChem–LETKF), the atmospheric CO_2 observations, and specifications of prior fluxes and uncertainties. Further details of the methodology are presented in the Appendix. In Sect. 3 we present GEOSChem–LETKF assessments of alternative specifications of ocean prior fluxes and flux uncertainties, and then use these results to derive long term estimates of North Atlantic CO_2 fluxes for the 2000–2017 period. We also summarize specific characteristics of North Atlantic CO_2 fluxes derived from these analyses, namely, long term means, trends, and interannual variability of fluxes, and compare our results with other recent relevant studies.

~~We investigate the sensitivity of the derived posterior flux estimates to three different representations of the ocean prior flux distribution and investigate an alternative method to characterize prior ocean flux uncertainty based on the ensemble spread of the multiple prior ocean fluxes. We derive North Atlantic CO_2 flux estimates for the 2000–2017 period and compare their characteristics with previous relevant studies.~~

2 Materials and Methods

2.1 Overview

Our analysis employs ~~the Localised Ensemble Kalman Filter (section 2.2) together with~~ the global GEOS-Chem atmospheric chemistry transport model together with the Localised Ensemble Kalman Filter (LETKF) (described in Ssect.~~ion~~ 2.~~3~~2) and atmospheric CO_2 observations from the NOAA-ESRL network of surface sites (~~section~~ Sect. 2.~~4~~3). Section 2.~~5~~ 4 describes the compilation of the set of air–sea CO_2 flux products and the derivation of the prior~~specification of~~ flux uncertainty specification for the North Atlantic based on the ensemble spread of these products. ~~multiple~~ Section 3 presents model results, including sensitivity analyses assessing different prior flux representations and flux uncertainty schemes (Sect. 3.1), and regional CO_2 flux estimates for the 2000–2017 period from the GEOSChem–LETKF system (Sect. 3.2). ~~representations of prior ocean fluxes (spread-based uncertainty). Section 2.6 presents sensitivity analyses assessing different prior flux representations and flux uncertainties defined from three different schemes (i.e., percentage-based uncertainty specifications (60%, 120%), and the spread-based uncertainty scheme).~~ Further details on the methods, model, observations and uncertainty calculations are presented in the sections below and in the Appendix.

Formatted: Subscript

2.2 2 The GEOSChem–Localized Ensemble Kalman Filter (GCL) system ~~Localized Ensemble Transform Kalman Filter (LETKF)~~

The GEOS−Chem atmospheric chemistry transport model has been used in a range of previous investigations into atmospheric CO_2 and applied in conjunction with inverse analyses to estimate surface carbon fluxes (Nassar et al., 2010, 2011; Suntharalingam et al., 2005; Liu et al., 2016). In this analysis we employ GEOSChem v11−01 at a horizontal resolution of 2° latitude by 2.5° longitude, with 47 levels in the vertical. Model transport fields are provided by GEOS-5 assimilated meteorological data from the NASA Global Modeling and Assimilation Office (GMAO, Rienecker et al., 2008). The GEOSChem configuration employed here primarily follows that of Nassar et al. (2011), but with updated representation of prior fluxes; more detail on the prior CO_2 fluxes and uncertainties implemented in this study is given in Sect. 2.4.

The Localized Ensemble Transform Kalman Filter (LETKF) is a data assimilation system which provides an estimate given a prior (or "background") estimate of the current state based on past and current data (in this case, the atmospheric CO_2 mole fraction observations). The general framework of the LETKF is described in Hunt et al. (2007); it has been adapted by Miyoshi et al. (2007) to provide gridscale localized analysis of flux estimates. The LETKF system has been used to estimate CO_2 fluxes in a range of previous studies (e.g, Kang et al., 2012; Liu et al., 2016, 2019).

The LETKF provides iterative estimates of the time evolution of the system state, x, (here representing the grid-scale surface carbon fluxes) ~~the gridscale surface carbon fluxes). Each step involves a forecast stage (based on a physical model of the system evolution) and a state estimation stage (the 'analysis' step), which combines system observations, y, together with the background forecast, x^b, to derive the improved state estimate. The observation operator H provides the mapping from the state space to the observation space; in this study H is provided by the GEOS−Chem atmospheric model (section 2.3).~~ Each step involves a forecast stage (based on a physical model of the system evolution) and a state estimation stage (the 'analysis' step), which combines system observations, y, together with the background forecast, x^b, to derive the improved state estimate. The observation operator H provides the mapping from the state space to the observation space; in this study H is provided by the GEOS–Chem atmospheric model.

In this analysis we employ the complete GEOSChem–LETKF (GCL) data assimilation system to conduct sensitivity analyses on the ocean prior fluxes, and to provide a long term flux estimate of surface CO_2 fluxes for the North Atlantic for the period 2000–2017. We report a posteriori fluxes on monthly timescales for the 2000–2017 period; the optimized monthly fluxes are derived from four sequential weeks of assimilation cycles, as further described below. Our methods follow the implementation of the LETKF system by Liu et al. (2019), who have extended the previous carbon data assimilation system of Kang et al. (2011, 2012). The study of Kang et al. (2011) assimilated meteorological data and atmospheric CO_2 concentrations to provide estimated atmospheric CO_2 concentrations as part of the state estimate. Kang et al. (2012) extended this method to also provide estimates of surface carbon fluxes. Both these LETKF studies assimilated meteorological data and atmospheric CO_2 concentrations and employed a short assimilation window of 6 hours in order to maintain linear behaviour of the ensemble

Formatted: Font: Bold, Font color: Auto

Formatted: Normal

Formatted: Font: 10 pt

perturbations (Kang et al., 2011, 2012). In addition, Kang et al. (2012) also tested longer assimilation windows (up to 3 weeks) for LETKF formulations that assimilated atmospheric CO_2 concentrations alone (eliminating the assimilation of the meteorological data). The LETKF system of Liu et al. (2019) extended the Kang et al. (2011, 2012) analyses by incorporating the GEOSChem atmospheric model as the forecast model, along with its representation of surface CO_2 fluxes which provide the prior flux specification for the forecast step. However, Liu et al. (2019) assimilate only atmospheric CO_2 measurements (i.e., no assimilation of meteorological measurements), and use an assimilation window of 7 days; the duration of the assimilation window was selected to maximize the correlation between observations and surface fluxes. The GEOSChem–LETKF system employed in our study follows the Liu et al. (2019) formulation; atmospheric CO_2 measurements are assimilated at 7 day timescales, with the LETKF analysis step providing updates of the surface fluxes and associated uncertainties required as initial conditions for the next weekly forecast step. We report monthly flux estimates following four assimilation cycles. Further details on the LETKF and the governing equations for flux estimation are provided in Appendix A.

~~Further details on the LETKF and the governing equations for flux estimation are provided in the Appendix A1.~~

~~In this analysis, the LETKF is used to derive gridscale fluxes for the period 2000–2017. The gridded fluxes are updated sequentially on weekly timescale by assimilation of the atmospheric CO_2 observations from a network of surface sites (section 2.4). We report a posteriori fluxes on monthly timescales for the 2000–2017 period; the optimized monthly fluxes are derived from four sequential weeks of assimilation cycles.~~

~~**2.3 The GEOS–Chem atmospheric transport model**~~

~~The GEOS–Chem atmospheric chemistry transport model has been used in a range of previous investigations into atmospheric CO_2 and applied in conjunction with inverse analyses to estimate surface carbon fluxes (Nassar et al., 2010, 2011; Suntharalingam et al., 2005; Liu et al., 2016). In this analysis we employ GEOSChem v11–01 at a horizontal resolution of 2° latitude by 2.5° longitude, with 47 levels in the vertical. Model transport fields are provided by GEOS–5 assimilated meteorological data from the NASA Global Modeling and Assimilation Office (GMAO, Rienecker et al., 2008). A detailed information of prior fluxes and uncertainties used in this study is given in Section 2.5.~~

2.~~4~~ 3 Atmospheric CO_2 Observations

Atmospheric CO_2 observations used for this study are taken from the NOAA–ESRL GLOBALVIEWplus Observation Package v4.2 (Obspack, Cooperative Global Atmospheric Data Integration Project, 2018). CO_2 measurement records for the period 2000–2017 from 86 surface sites were used in this analysis. Further details on the measurement sites and the site–specific observation uncertainty characteristics are presented in Table A1 of the Appendix. The specification of observational uncertainty associated with incorporation of the atmospheric CO_2 measurements into the LETKF is derived using the methods of Chevallier et al. (2010); we use the standard deviation of measurement variability from detrended and deseasonalized CO_2 time series at each measurement site. The resulting specification of observational uncertainty varies between 0.16 ppm (for

stations in and around the Southern Ocean) to over 5 ppm (for stations in continental interiors) (see Appendix Table A1 for more details).

2.~~5~~ 4 Specification of Prior CO_2 Fluxes and Associated Flux Uncertainties

The GEOSChem model CO_2 simulation employed in this study includes representation of fossil fuel emissions, air–sea fluxes and exchange with the terrestrial biosphere. Details of the data sources used to specify the prior flux distributions are outlined here. ~~A priori CO_2 flux distributions implemented in the GEOS−Chem model for this analysis include~~ Ffossil fuel emissions are taken from Chevallier et al. (2019) (Global Atmospheric Research version 4.3.2, Crippa et al., 2016, scaled globally and annually from Le Quéré et al., 2018), and land biosphere fluxes from the Joint UK Land Environment Simulator (JULES, Clark et al., 2011).

The focus of our study is on North Atlantic Ocean CO_2 fluxes, and we investigate the representation of ocean prior fluxes and prior flux uncertainty in more detail. Firstly, in Sect. 3.1, in a set of sensitivity analyses, we compare the implementation of three different representations of ocean CO_2 fluxes that have been used to specify prior fluxes in recent inverse analyses: (i) the widely used ~~We evaluate three separate representations for ocean CO_2 fluxes, namely,~~ Takahashi et al. (2009) climatology (hereinafter Ta), (ii) the interannually varying flux product of Landschützer et al. (2016) derived from surface pCO_2 distributions (hereinafter La), and (iii) the interannual fluxes from the ocean mixed-layer scheme of Rödenbeck et al. (~~2013~~2014) (hereinafter Ro). We also evaluate in more detail, the impact of different specifications of prior flux uncertainty for ocean fluxes. Many previous atmospheric inverse estimates of air–sea carbon fluxes have employed relatively simple characterizations of the prior ocean flux uncertainty, for example, based on a fixed proportion of the grid–scale or regional prior flux (Nassar et al., 2011, Liu et al., 2016, Feng et al., 2016). In Sect. 3.1, we employ both fixed flux uncertainties, and also present an alternative scheme derived from the ensemble spread of ocean CO_2 flux products, as described below.

The prior ocean flux distributions employed in atmospheric inversions are frequently derived from interpolations of the surface ocean pCO_2 database (e.g., SOCAT, Bakker et al., 2016) in combination with ocean–atmosphere gas exchange parameterizations. Uncertainties in the derived products stem from uncertainties in the input data (e.g., density of measurements), interpolation methods, and gas–transfer parameterizations (Landschutzer et al., 2013). However, some ocean regions, the North Atlantic in particular, have a higher density of pCO_2 measurements and more consistent flux estimates from pCO_2–based products (Schuster et al., 2013, Landschutzer et al., 2013). Here we exploit the recent expansion of pCO_2–based ocean flux products to outline a new specification of ocean prior flux uncertainty based on the ensemble–spread of the different flux products (the "spread–based" uncertainty scheme). Towards the development of the spread–based scheme, we have compiled a set of eight global gridded interannually varying ocean–atmosphere CO_2 flux products. These are Landschutzer et al., 2016, Rodenbeck et al., 2014, Denvil–Sommer et al., 2019, Iida et al., 2015, Zeng et al., 2015, Gregor et al., 2019, Chau et al., 2020, and Watson et al., 2020.

~~Since the primary focus of our investigation is to estimate North Atlantic Ocean CO_2 fluxes, we have evaluated in more detail, the impact of different specifications of prior flux uncertainty for ocean fluxes. Specifications of prior flux uncertainty for~~

~~ocean fluxes include (a) a percentage based level (U1:60% of prior flux, and U2:120% of prior flux), and (b) gridded flux uncertainties representing the variation or 'spread' of the different ocean flux data products at each location~~The ~~, and based on the standard deviation of the variation among the prior fluxes (U3:~~ spread~~ -~~based prior flux uncertainty scheme uses a diagnostic derived from the variation among the set of ocean atmosphere carbon flux products (~~;~~ see ~~Eq. (equation~~ 1)). This scheme specifies lower uncertainty levels where alternative prior flux representations are in accord (e.g., when well–constrained by availability of surface pCO_2 measurements), and higher uncertainty levels where the prior flux distributions differ significantly (typically in under–sampled regions or those of significant flux variability). This specification follows previously used methods to characterize uncertainties in ocean flux distributions (e.g., Bopp et al., 2013). For this spread–based uncertainty specification~~latter specification (U3)~~, the gridded prior flux uncertainty, *U(i,j)* (for a gridcell with coordinates *(i,j)*) is specified as the standard deviation of the spread of the ~~-~~different prior flux products. Thus, the uncertainty *U(i,j)* is calculated as:

$$U(i,j) = sqrt(\sum_{k}^{K} \left(f_k(i,j) - \overline{f(i,j)}\right)^2)/(K-1) \quad (1)$$

Here K is the total number of the prior ocean flux products considered, and subscript k refers to an individual flux product. $f_k(i,j)$ represents the gridded monthly flux for each prior ocean flux and $\overline{f(i,j)}$ is the gridded monthly mean across all prior ocean flux products. These prior flux uncertainties are estimated on monthly timescales and also account for interannual variations. The uncertainty statistics of the prior ocean flux distributions will be dependent on the uncertainties associated with the respective inputs and methods of constructing the flux products. Ocean–atmosphere carbon flux products derived from surface ocean pCO_2 measurements are generally subject to two main sources of uncertainty: (i) in the specification of the surface CO_2 partial pressure difference across the air–sea interface, and (ii) in the specification of the gas–exchange coefficient used to derive fluxes (e.g., see discussion of Landschutzer et al., 2013; Watson et al., 2020). In the extended database of 8 pCO_2–based flux products that we present above, the majority of the flux products (seven of the eight) rely on the surface ocean pCO_2 data of the SOCAT database (Bakker et al., 2016). These flux products will be subject to similar uncertainties associated with data coverage in different ocean regions, although the uncertainties due to differences among surface interpolation methods may vary.

In this study we account for spatial correlations in the prior ocean fluxes, by inclusion of off diagonal elements in the background error covariance matrix P^b (Appendix A1 Eq. A3). We follow the recommendations of Jones et al. (2012) on autocorrelation length scales in the surface ocean. That study derived spatial autocorrelation functions for air–sea fluxes from an analysis of the surface ocean pCO_2 database reported in Takahashi et al. (2009), combined with a gas exchange

parameterization. We currently do not account for spatial correlation in land fluxes, but will investigate this in future analyses. ~~The representation of ocean prior flux uncertainty is further discussed in section 3.1.~~

Formatted: English (United States), Kern at 14 pt

3 Results and Discussion

We first present in Sect. 3.1 results of short–term sensitivity tests that compare the influence of ~~Section 3.1 and Table 1 present sensitivity tests conducted for~~ different prior ocean flux distributions and prior ocean flux uncertainty schemes on GCL estimates of North Atlantic (NA) CO_2 fluxes. Using these analyses as a basis,~~.~~ in Sect.~~ion~~ 3.2 we conduct a multi–year GCL analysis ~~presents the estimates~~ of North Atlantic CO_2 ocean fluxes for the 2000–2017 period. We also report on derived characteristics of regionally aggregated North Atlantic subtropical and subpolar fluxes (long term means, trends and interannual variability) and compare these GCL results with recent estimates from other methodologies, including global ocean biogeochemical models (GOBMs), other atmospheric inverse studies, and surface pCO_2–based data products.~~We focus on the long term mean values, interannual variability and trends of the GCL estimates of CO_2 ocean fluxes. In section 3.2 we also compare the results from this study with previous estimates of North Atlantic (NA) fluxes.~~

3.1 Sensitivity tests on specification of prior flux uncertainty

In this section we investigate, via sensitivity analyses, the application of the spread–based prior flux uncertainty scheme outlined in Sect. 2.4 in comparison to the fixed prior uncertainty levels commonly used in previous inverse estimates of ocean CO_2 fluxes. The alternative specifications of prior flux uncertainty for ocean fluxes employed include (a) fixed percentage-based levels (U1:60% of prior flux, and U2:120% of prior flux), and (b) gridded flux uncertainties representing the variation or 'spread' of the different ocean flux data products at each location, and based on the standard deviation of the variation among the prior fluxes (U3: spread–based uncertainty; see Eq. (1)). The selection of the fixed percentage prior uncertainty levels used in the sensitivity analyses was based on the range of variability seen for the individual prior flux distributions (Fig. 1) for the sub–regions of the North Atlantic. These ranged from average levels of ~60% for the subtropical North Atlantic to levels greater than 120% for the subpolar North Atlantic, hence we have selected a level of U1:60% to characterize the lower sensitivity case, and U2:120% for the higher case. We apply the alternative flux uncertainty specifications to the three different ocean prior flux distributions discussed in Sect. 2.4, namely: (i) the Takahashi et al. (2009) climatology (Ta), (ii) the flux product of Landschützer et al. (2016) (La), and (iii) the flux product of Rödenbeck et al. (2014) (Ro).

~~We first assess the sensitivity of derived flux estimates to the specification of prior flux uncertainty;~~ Sensitivity~~this~~ analyses are~~is is~~ conducted for the year 2003, following a 3 year GEOSChem model spin–up, starting from January 1st, 2000; the length of spin–up was determined by recommendations on the duration required for stabilization of tropospheric CO_2 gradients (e.g., Gurney et al., 2002), and following methods used for previous GEOSChem CO_2 analyses (e.g., Nassar et al., 2010). The year 2003 was selected for sensitivity tests as the first viable year following spin–up. Analyses of inter–annual variability in Atlantic CO_2 (e.g., Landschutzer et al., 2013; Schuster et al., 2013) do not find 2003 to be an anomalous year for regional ocean fluxes.

~~. An initial three year model spin-up, starting from January 1st, 2000 was conducted following the CO_2 simulation and methods of Nassar et al. (2010).~~ We evaluate the sensitivity of posterior ocean flux estimates with three different prior ocean uncertainty schemes U1, U2, and U3, described ~~in section 2.5~~above; these are applied in turn for each of the three prior ocean flux distributions (Ta, La and Ro). Figure 1 presents the seasonal variation ~~an example distribution~~ of the spatial distribution of the spread-based prior ocean flux uncertainty U3 (~~shown as a quarterly~~ 3 month averages for ~~an example~~the year of 2003). Figure 1 demonstrates that over the course of the year, and particularly in the Northern Hemisphere winter months, the spread-based uncertainty scheme (U3) provides a looser constraint on prior fluxes (i.e., levels of prior flux uncertainty > 120%) than the U1 and U2 schemes in the subpolar region, and a tighter constraint in the subtropical region (levels < 60%).

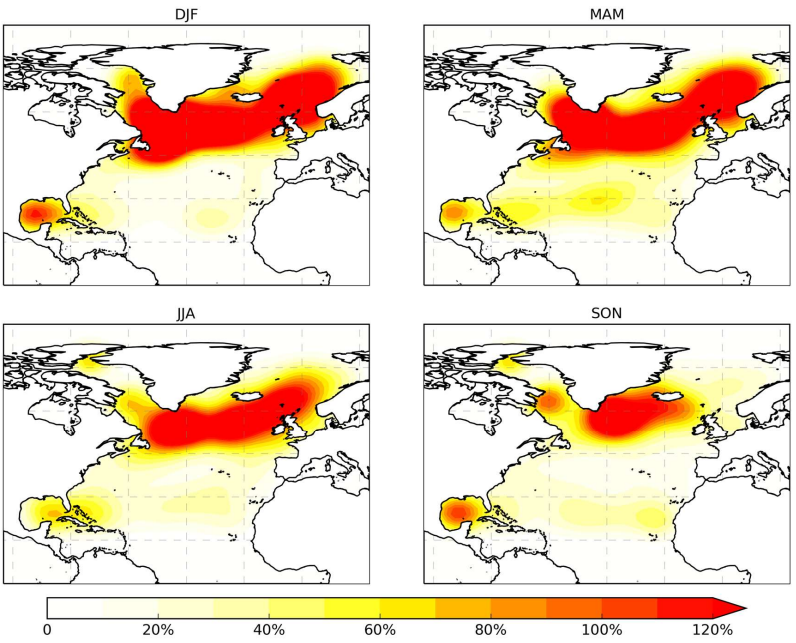
DJF
MAM
JJA
SON
0
20%
40%
60%
80%
100%
120%

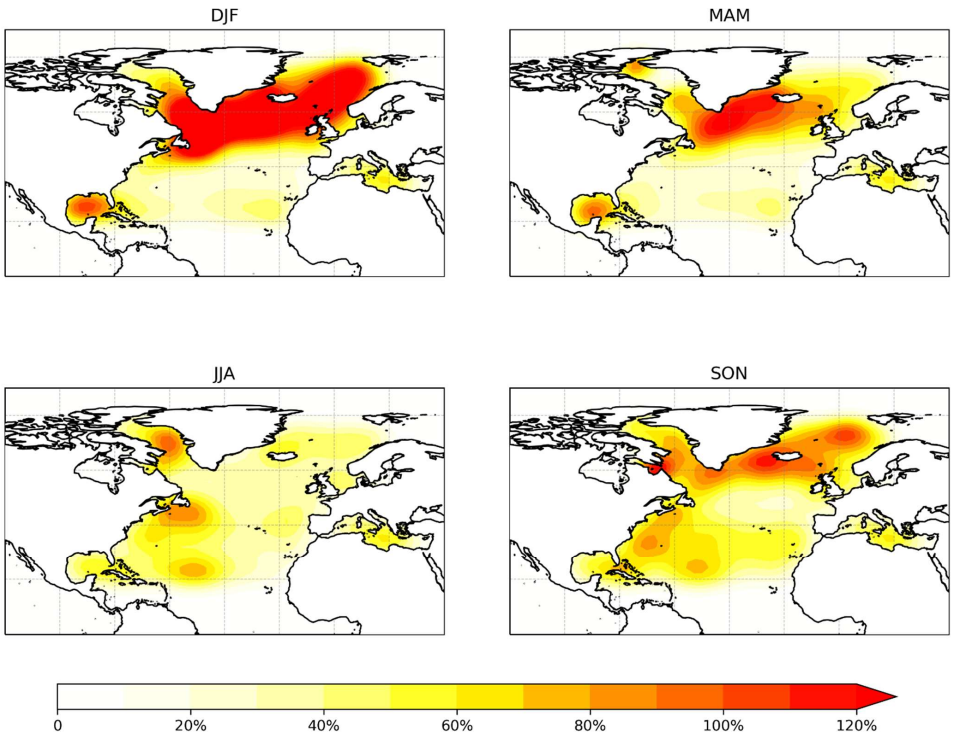

Figure 1. Distribution of the spread–-based prior ocean flux uncertainty (U3) (3 month~~annual~~ averages for the year 2003). The distribution in this study is calculated from the following 8 air–sea CO_2 flux products: (1) Denvil–Sommer et al., 2019 (product LSCE–FFNN–v1); (2) Iida et al., 2015 (JMA); (3) Zeng et al., 2015 (NIES); (4) Gregor et al., 2019 (CSIR–ML6); (5) Chau et al., 2020 (CMEMS); (6) Watson et al., 2020; (7) Landschützer et al., 2016; (8) Rödenbeck et al., 2014. It is represented here as a percentage of the prior ocean flux for ease of comparison with U1 and U2. The percentage shown for each grid–-cell is derived from the ratio of spread−based prior ocean uncertainty divided by the prior ocean flux value at that grid cell. DJF represents the monthly average for December, January, February; MAM for March, April, May; JJA for June, July, August; SON for September, October, November.

Table 1 summarizes the prior and posterior ocean flux estimates for the global and North Atlantic region (sub–-divided into subpolar and subtropical regions) from the respective sensitivity tests. The distribution of prior flux for the subtropical North Atlantic shows closer agreement among the three source representations (Ta, La and Ro), with regional variation of 0.05 PgC y^{-1}, in comparison to a regional variation of ~0.1 PgC y^{-1} for the subpolar region.

Under the constraints provided by the atmospheric CO_2 observations all posterior flux estimates for the North Atlantic show increased uptake (Table 1), indicating that all three representations of ocean prior flux underestimate the regional net atmosphere–ocean flux for the 2003 period. Largest changes in the regional posterior fluxes are estimated under the U3 specification of prior flux uncertainty. In addition, Our our estimates indicate a larger increase in CO_2 uptake in the subpolar basin (~0.05 05 PgC y^{-1}, changing from a prior flux range of -0.13 to -0.23 PgC y^{-1} to posterior flux range of -0.189 to -0.28 27 PgC y^{-1}, for the U3 scenarios), in comparison to the smaller magnitude change for the subtropical North Atlantic basin (of ~ 0.02 04 PgC y^{-1} from -0.17 to -0.22 PgC y^{-1} to -0.22 to -0.25 26 PgC y^{-1} for the U3 scenarios)

Table 1. Global and North Atlantic CO_2 flux estimates from the GEOSChem−LETKF(GCL) system for year 2003 (PgC y^{-1}) summarizing sensitivity analyses on the prior ocean flux distribution and prior flux uncertainty. Prior flux references are Ta: Takahashi et al. 2009; La: Landschutzer et al. 20172016; Ro: Rodenbeck et al. 20132014. Prior flux uncertainty specifications are: U1: 60%; U2: 120%: U3: spread−based (following methods of Ssect ion 2.54).

Global Ocean CO_2 Flux (PgC y^{-1})					
Ta	-1.37	La	-1.25	Ro	-2.09
TaU1	-1.63±0.13	LaU1	-1.52±0.13	RoU1	-2.31±0.16
TaU2	-2.05±0.26	LaU2	-1.96±0.26	RoU2	-2.68±0.31
TaU3	- 2.241.97±0.1728	LaU3	- 1.832.21±0.1928	RoU3	- 2.6073±0.128
North Atlantic subtropics [15°N–50°N]					
Ta	-0.22	La	-0.18	Ro	-0.17
TaU1	-0.23±0.02	LaU1	-0.19±0.02	RoU1	-0.18±0.02
TaU2	-0.25±0.05	LaU2	-0.21±0.04	RoU2	-0.20±0.04
TaU3	-0.264±0.035	LaU3	-0.220±0.035	RoU3	- 0.2319±0.035
North Atlantic subpolar [50°N–80°N], west eastern boundary atof 20°E					
Ta	-0.23	La	-0.13	Ro	-0.21
TaU1	-0.23±0.05	LaU1	-0.13±0.02	RoU1	-0.22±0.04
TaU2	-0.25±0.1	LaU2	-0.14±0.05	RoU2	-0.23±0.09
TaU3	-0.278±0.0511	LaU3	-0.189±0.0511	RoU3	- 0.246±0.0511

We note that the increases in estimated uptake for the North Atlantic basins are relatively smaller (on average in the range 10−20%) than the increased uptake estimated on the global scale (~30−7050% changes, see Table 1), indicating that prior flux representations of the North Atlantic carbon uptake are more consistent with the constraints from atmospheric CO_2 measurements than those for other regions of the global ocean.

The U3 flux uncertainty specification is derived from the variation among a set of ocean–atmosphere carbon flux products (Eq. (1)). This scheme specifies lower uncertainty levels where alternative prior flux representations are in accord (e.g., when well constrained by availability of surface pCO_2 measurements, as in the subtropical North Atlantic), and higher uncertainty levels where the prior flux distributions differ significantly (typically in under–sampled regions or those of significant flux variability, such as the subpolar North Atlantic). We further assess the value of the U3 scheme using a metric of GCL modeled atmospheric CO_2 concentration; specifically, estimates of the model–observation mismatch for the year 2003 at the NOAA network station sites in the North Atlantic using the a posteriori fluxes associated with the sensitivity analyses of this section (Appendix Table A2). The results summarized in Table A2 indicates that scheme U3 provides the smallest magnitude model-observation mismatch for the individual North Atlantic sites and for the global network average. ~~Use of the spread–based uncertainty scheme (U3) enables flexibility in specification of the regional magnitude of the prior flux uncertainty, as it allows tighter constraints in regions where alternative prior flux representations are in accord, and looser constraints in regions where prior flux representations differ significantly.~~ For the long term analyses of the remainder of this study, ~~we~~ therefore, we use the U3 spread–based flux uncertainty scheme in preference to the fixed level flux uncertainty schemes used in many previous inverse analyses.

~~. We will also employ the flux distribution of Landschützer et al. (2016) as the prior flux distribution as it provides interannually varying fluxes over the entire estimation period (2000–2017).~~

3.2 Multi-year analyses of North Atlantic CO_2 fluxes

In this section we present results of a multi-year GCL analysis (for the period 2000–2017), calculating~~assessing~~ regional estimates of North Atlantic CO_2 fluxes on annual to decadal timescales. Prior flux distributions for fossil emissions, and exchange with the land biosphere fluxes are as described in Sect. 2.4. For ocean prior fluxes, we employ the distribution of Landschützer et al. (2016); this is an established surface pCO_2-based product and also provides inter-annually varying fluxes over the entire estimation period (2000–2017), in comparison to the climatology-only fluxes of Takahashi et al. (2009). Ocean prior flux uncertainties are specified by the spread-based scheme U3 described above and derived from the eight ocean–atmosphere pCO_2–based flux products summarized in Sect. 2.4. ~~We assess the GCL a posteriori estimates of ocean fluxes using the prior flux specifications outlined in section 2; i.e., La, Ro and Ta. All other prior flux distributions (for fossil emissions, and land biosphere fluxes) are as described in section 2.4. To evaluate the inverse results in this study further, we compare our results with the estimates from three other inverse systems including CAMS (v18r2, Chevallier et al., 2019), CT (CarbonTracker 2019, Jacobson et al., 2020) and CTE (Carbon Tracker Europe, van der Laan-Luijkx et al., 2017). All data are regridded to 2° latitude × 2.5° longitude to be consistent with the GCL model resolution.~~

Formatted: Font: 12 pt

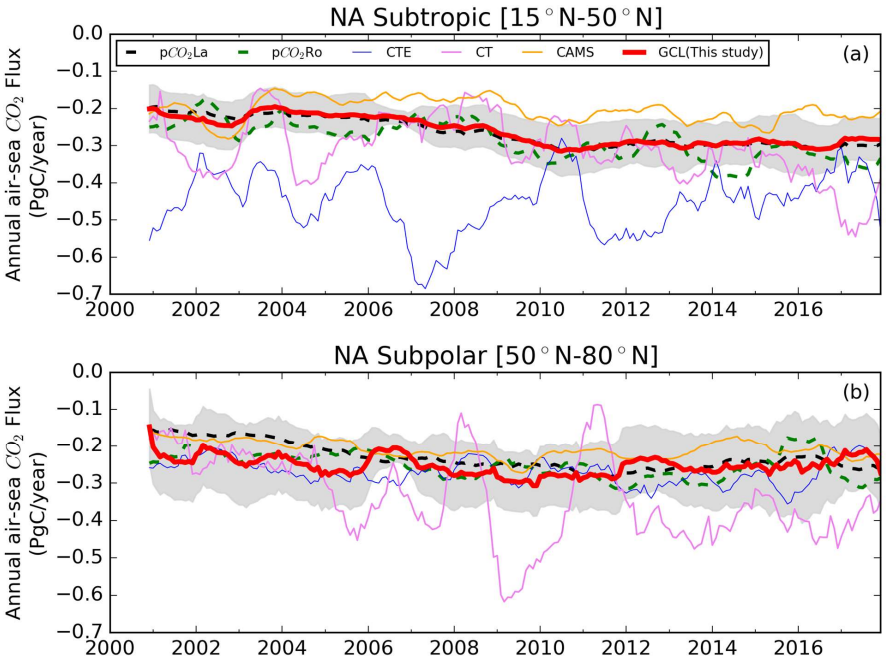
NA Subtropic [15°N-50°N]
pCO2La
pCO2Ro
CTE
CT
CAMS
GCL(This study)
(a)
Annual air-sea CO2 Flux (PgC/year)
0.0
−0.1
−0.2
−0.3
−0.4
−0.5
−0.6
−0.7
2000
2002
2004
2006
2008
2010
2012
2014
2016
NA Subpolar [50°N-80°N]
(b)

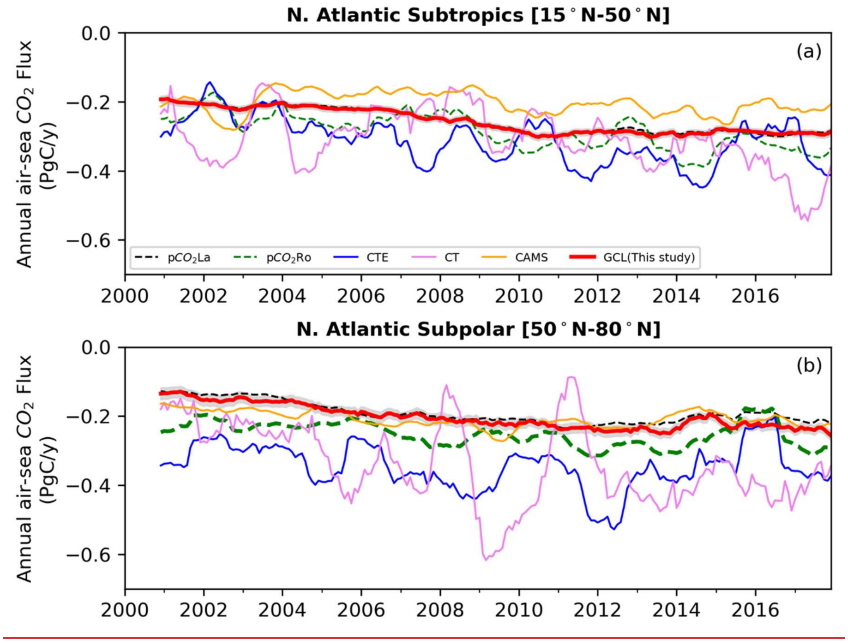

355

Figure 2. Comparison of annual air−sea CO_2 fluxes for North Atlantic for the 2000−2017 period for: (a) North Atlantic Subtropics; and (b) North Atlantic Subpolar regions. The GCL posterior flux estimate from this study (red) is derived from the prior flux of Landschützer et al., 2016 (pCO_2La: black). The grey shaded area represents the uncertainty estimate on the GCL posterior flux (plotted at a ~~3~~ 1 sigma level). Also shown are the flux estimates of (i) Chevallier et al., 2019 (CAMS: yellow); (ii) Jacobson et al., 2020 (CT: CarbonTracker2019: pink); and (iii) van der Laan−Luijkx et al., 2017 (CTE: Carbon Tracker Europe: blue). All time series shown have a 12 month running mean filter applied.

Figure 2 presents the variation of air−sea CO_2 flux for the North Atlantic subtropical and subpolar regions for the 2000−2017 period (represented as a 12 month running average). ~~,~~ We also plot on Fig. 2 flux estimates from three other atmospheric inverse analysis studies including CAMS (v18r2, Chevallier et al., 2019), CT (CarbonTracker 2019, Jacobson et al., 2020) and CTE (Carbon Tracker Europe, van der Laan–Luijkx et al., 2017). All data are regridded to 2° latitude × 2.5° longitude to be consistent with the GCL model resolution. ~~and comparison to estimates from previous studies.~~

For the North Atlantic subtropical region, the GCL posterior flux magnitude is ~~similar~~ close to that of the ocean prior flux employed (Landschutzer et al., 2016), with a difference of approximately ~~less than~~ 0.~~02~~ 01 PgC y^{-1} over the period. Variation among the other inverse flux estimates can reach up to 0.~~5~~ 3 PgC y^{-1} (e.g., between CT~~E~~ and CAMS in 2007), and these

differences can be ascribed, in part, to the different underlying prior flux distributions used in the respective inverse analyses (see Sect. 3.2.2). ~~These larger variations primarily result from the different prior ocean fluxes used in the respective inverse studies. This issue has been previously noted by other studies; e.g., Nassar et al. (2011), note that that the prior ocean flux used in CTE (Jacobson et al., 2007; van der Laan–Luijkx et al., 2017) provides approximately 85% more carbon uptake (on a global basis) than the ocean flux estimates of Takahashi et al. (2009).~~

For the North Atlantic subpolar region, the GCL posterior flux estimate deviates more from the prior flux estimate (e.g., showing differences of up to 0.~~09~~ 04 PgC y^{-1}), especially ~~in the early decade of the analysis~~for some years (201200 – 201~~70~~) of the analysis. The majority of flux estimates for the North Atlantic subpolar region are in closer accord (Fig. 2b) with differences of less than 0.2 PgC y^{-1} (the CT estimate is an exception indicating variations of greater than 0.3 PgC y^{-1} from the other estimates). A potential reason for the anomalous behaviour of the CT estimate in the North Atlantic is the underlying prior flux uncertainties used in the analysis which give a loose constraint on the prior ocean fluxes and allow the ocean fluxes deviate far from the prior because of the impaction from atmospheric CO_2 signals.

We also note that Peylin et al. (2013) have suggested that significant inter–annual variability in atmospheric inverse estimates is a potential indicator of 'flux leakage', where significant variability of terrestrial carbon fluxes in combination with sparse atmospheric sampling can result in misattribution of carbon flux estimates between land and ocean. To assess the significance of flux leakage in our GCL analyses, we have calculated estimates of the diagnostic recommended by Peylin et al. (2013) (i.e., the correlation between the annual total land and total ocean fluxes) for the Northern Hemisphere as a whole (Equator to 90°N), and also by latitudinal region. Estimates of this diagnostic are relatively low for our GCL analyses (values of 0.2 and 0.5 for the subpolar and subtropical regions) indicating low potential for flux leakage. As a point of comparison, Peylin et al. (2013) note that six out of eleven atmospheric inverse analyses in their model inter–comparison reported correlation coefficients of greater than 0.5.

~~The long-term mean, IAV and trends of these estimates are discussed in the following subsections.~~

3.2.1 Long term mean

Figure 3 provides a comparison of the following GCL flux estimates and associated characteristics for the North Atlantic subtropical and subpolar regions for the period 2000 – 2017: (i) the long term mean of air – sea CO_2 flux estimates (~~The~~ the underlying data are tabulated in Table 2); (ii) the ~~amplitude of~~ estimated inter–annual variability (IAV) of fluxes (Table 3); and (iii) the long term trends (Table 4). The IAV is calculated following methods of Rödenbeck et al. (2015) (i.e., derived from the standard deviation of the residuals of a 12 month running mean over the CO_2 flux time series).

Formatted: Font: (Default) +Body (Times New Roman)

Formatted: Font: (Default) +Body (Times New Roman)

Formatted: Font: (Default) +Body (Times New Roman)

Formatted: Font: (Default) +Body (Times New Roman)

Formatted: Justified

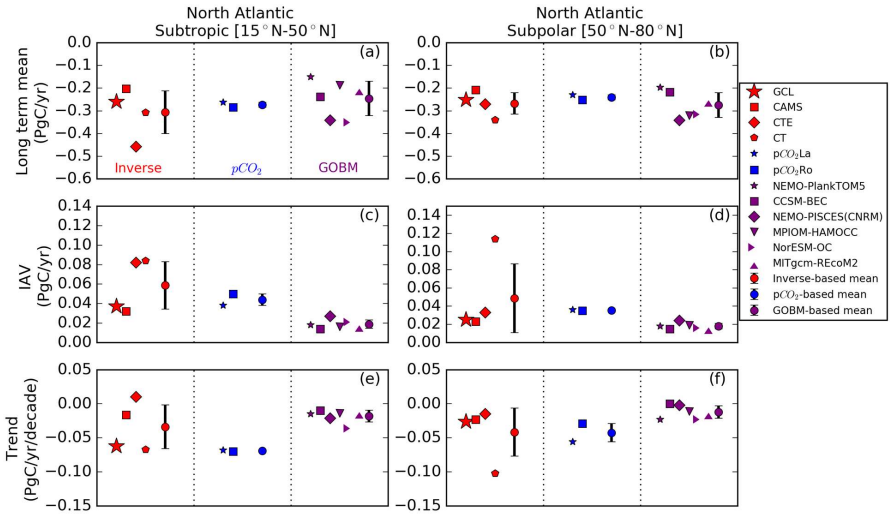
North Atlantic
Subtropic [15°N-50°N]
North Atlantic
Subpolar [50°N-80°N]
Long term mean (PgC/yr)
IAV (PgC/yr)
Trend (PgC/yr/decade)
Inverse
pCO_2
GOBM
(a)
(b)
(c)
(d)
(e)
(f)
GCL
CAMS
CTE
CT
pCO_2La
pCO_2Ro
NEMO-PlankTOM5
CCSM-BEC
NEMO-PISCES(CNRM)
MPIOM-HAMOCC
NorESM-OC
MITgcm-REcoM2
Inverse-based mean
pCO_2-based mean
GOBM-based mean

400

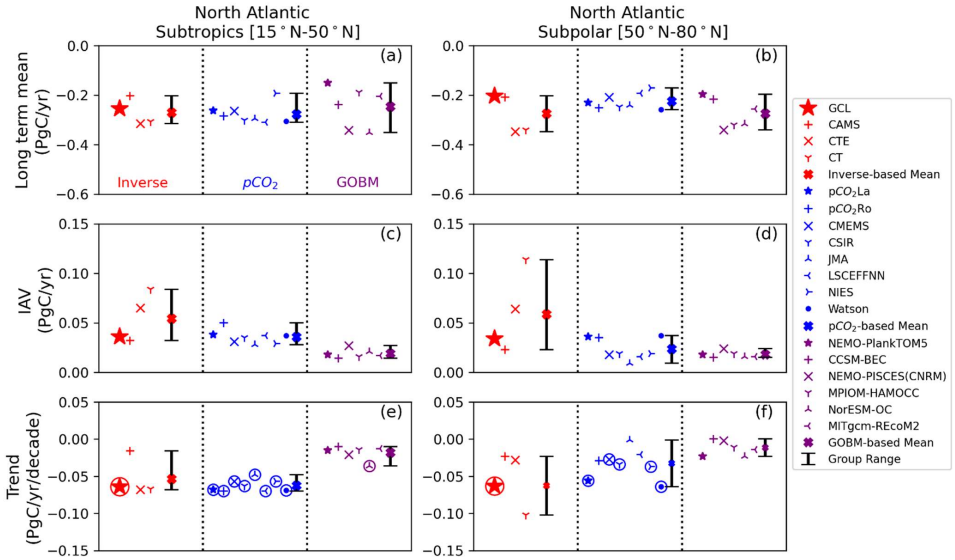
North Atlantic
Subtropics [15°N-50°N]
North Atlantic
Subpolar [50°N-80°N]
Long term mean (PgC/yr)
IAV (PgC/yr)
Trend (PgC/yr/decade)
Inverse
pCO_2
GOBM
(a)
(b)
(c)
(d)
(e)
(f)
GCL
CAMS
CTE
CT
Inverse-based Mean
pCO_2La
pCO_2Ro
CMEMS
CSIR
JMA
LSCEFFNN
NIES
Watson
pCO_2-based Mean
NEMO-PlankTOM5
CCSM-BEC
NEMO-PISCES(CNRM)
MPIOM-HAMOCC
NorESM-OC
MITgcm-REcoM2
GOBM-based Mean
Group Range

Figure 3. Comparison of CO_2 ocean flux metrics for the 2000–2017 period for North Atlantic subtropics (left panels) and subpolar regions (right panels). Metrics shown are the long term mean (panels (a) and (b)); interannual variability (IAV) (panels (c) and (d)); and long term trend (panels (e) and (f)). The GCL estimates (red stars) are shown in comparison to other atmospheric inverse analyses (red symbols), surface ocean pCO_2 products (blue) and global ocean biogeochemistry models (GOBMs, purple). Also shown are the estimated mean valuess from each sub-group of analyses (filled cross ~~circle~~ symbols) with their minimum–maximum range. Circled symbols in panel (e) and (f) indicate a statistically significant trend.~~associated uncertainty (1 standard deviation).~~

Formatted: Strikethrough

Table 2. Summary metrics of GEOSChem–LETKF North Atlantic (NA) CO_2 flux estimates, and comparison with independent estimates (from atmospheric inverse analyses, surface pCO_2 mappings, and Global Ocean Biogeochemistry models (GOBMs)) for the period 2000–2017. Listed are estimates for the long term mean. The metrics listed in this table are plotted in Fig. 3a and 3b.

Long term mean (PgC y^{-1})		
NA Subtropics (15°N–50°N)	**NA Subpolar** (50°N–80°N; eastern boundary at 20°E)	
Atmospheric inversions		
-0.255±0.037	*-0.203±0.037*	*This study (GCL)*[a]
-0.203	-0.208	CAMS (Chevallier et al. 2019)
-0.315	-0.347	CTE (van der Laan–Luijkx et al. 2017)
-0.307	-0.340	CT (Jacobson et al. 2020)
[-0.315, -0.203]	[-0.347, -0.203]	Range of all atmospheric inverse studies (minimum to maximum)
Surface ocean pCO_2–based flux products		
-0.263	-0.230	pCO_2La (Landschutzer et al. 2016)
-0.284	-0.252	pCO_2Ro (Rodenbeck et al. 2014)
-0.264	-0.208	CMEMS (Chau et al. 2020)
-0.302	-0.248	CSIR (Gregor et al. 2019)
-0.295	-0.241	JMA (Iida et al. 2015)
-0.309	-0.192	LSCEFFNN (Denvil–Sommer et al. 2019)

-0.193	-0.171	NIES (Zeng et al. 2015)
-0.305	-0.259	Watson et al. (2020)
[-0.309, -0.193]	[-0.259, -0.171]	Range of all pCO_2–based representations (minimum to maximum)
Global ocean biogeochemistry models		
-0.150	-0.197	NEMO–PlankTOM5 (Buitenhuis et al. 2010)
-0.238	-0.217	CCSM–BEC (Doney et al. 2009)
-0.342	-0.341	NEMO–PISCES (CNRM) (Séférian et al. 2013)
-0.188	-0.321	MPIOM–HAMOCC (Ilyina et al. 2013)
-0.351	-0.316	NorESM–OC (Schwinger et al. 2016)
-0.205	-0.256	MITgcm–REcoM2 (Hauck et al. 2016)
[-0.351, -0.150]	[-0.341, -0.197]	Range of GOBM studies (minimum to maximum)
Long term mean (PgC y^{-1})		
NA Subtropics	**NA Subpolar**	
Atmospheric inversions		
-0.26±0.04	*-0.25±0.04*	*This study (GCL)*[a]
-0.203	-0.208	CAMS (Chevallier et al. 2019)
-0.457	-0.270	CTE (van der Laan–Luijkx et al. 2017)
-0.307	-0.34	CT (Jacobson et al. 2020)
-0.30±0.11	-0.26±0.05	Mean of all atmospheric inverse studies[b]
Surface ocean pCO_2-based flux products		
-0.263	-0.23	pCO_2La (Landschutzer et al. 2016)
-0.284	-0.252	pCO_2Ro (Rodenbeck et al. 2013)
-0.27±0.01	-0.24±0.01	Mean of all pCO_2-based representations[b]
Global ocean biogeochemistry models		
-0.150	-0.197	NEMO-PlankTOM5 (Buitenhuis et al. 2010)
-0.238	-0.217	CCSM-BEC (Doney et al. 2009)
-0.342	-0.341	NEMO-PISCES (CNRM) (Séférian et al. 2013)
-0.188	-0.321	MPIOM-HAMOCC (Ilyina et al. 2013)
-0.351	-0.316	NorESM-OC (Schwinger et al. 2016)
-0.205	-0.256	MITgcm-REcoM2 (Hauck et al. 2016)
-0.24±0.07	-0.27±0.05	Mean of GOBM studies[b]

Formatted Table

Formatted: Font: 10 pt, Bold

Formatted: Font: Bold

Formatted: Centered, Line spacing: single

Formatted: Left, Line spacing: single

[a] The uncertainty of the long term mean estimate from the GCL (this study) is calculated as the standard deviation of the annual flux estimates over the (2000–2017) period.

We also present in Fig. 3 the equivalent estimates from other independent assessments, including (i) other atmospheric inverse analyses, (ii) surface ocean pCO_2–based analyses, and (iii) analyses from global ocean biogeochemistry models (GOBMs)~~.,~~ ~~Buitenhuis et al., 2010; Doney et al., 2009; Séférian et al., 2013; Ilyina et al., 2013; Schwinger et al., 2016; Hauck et al., 2016).~~ For the North Atlantic subtropical region, the long term mean of the GCL posterior flux estimate is -0.~~26~~255±0.~~04~~ 037 PgC y^{-1} (Figure 3a and Table 2). It lies in the range spanned by the other inverse analyses (-0.31 to -0.20 PgC y^{-1}, of slightly larger magnitude than CAMS, but smaller than CT and CTE), and is in ~~This is consistent with the observationally-based "best" estimate of Schuster et al. (2013) for the period 1990-2009. Figure 3 (and Table 2) also indicate generally~~ good agreement with the mean~~–~~value estimates ~~between the GCL estimate for North Atlantic subtropical region fluxes and estimates~~ from surface pCO_2–based methods and GOBMs. For the North Atlantic subpolar region, the GCL estimate of the long term mean uptake is -0.203±0.037 PgC y^{-1} (Table 2), close to the inverse estimate of the CAMS analysis, and of smaller magnitude (by ~0.1 PgC y^{-1}) than the inverse estimates of CT and CTE. The GCL estimate is consistent with the mean estimate from pCO_2–based products, and within the range of flux estimates from GOBMs (from -0.341 to -0.197 PgC y^{-1}). ~~The GCL inverse estimate is also consistent with 2 of the other 3 inverse flux estimates considered, with only the flux estimate from CTE (van der Laan-Luijkx et al., 2017) significantly different with an uptake level greater than 0.4 PgC y^{-1}. For the North Atlantic subpolar region, the GCL estimate of the long term mean uptake is -0.25±0.04 PgC y^{-1} (Table 2), which is slightly larger than that of the prior flux (-0.23 PgC y^{-1}) and the estimate of -0.21 PgC y^{-1} from Schuster et al. (2013). The ensemble mean from each group (atmospheric inversions, pCO_2–based and GOBMs) agree well and range from -0.24 PgC y^{-1} to -0.27 PgC y^{-1}.~~

3.2.2 Interannual variability

The interannual variability (~~magnitude of~~ IAV) of CO_2 flux estimates derived from the GCL is 0.~~037~~036±0.006 PgC y^{-1} for the North Atlantic subtropics and 0.~~025~~034±0.009 PgC y^{-1} for the North Atlantic subpolar region (Fig. 3c and 3d, Table 3). The IAV estimates ~~for the NA subtropics~~ from the different inverse analyses for both the North Atlantic subtropics and subpolar regions display a large range ~~of values~~ (0.~~019~~032 to 0.~~059~~084 PgC y^{-1} and 0.023 to 0.114 PgC y^{-1} respectively), than the ranges displayed by GOBMs (0.014 to 0.027 PgC y^{-1} and 0.015 to 0.024 PgC y^{-1} respectively) and pCO_2–based fluxes (0.029 to 0.050 PgC y^{-1} and 0.009 to 0.037 PgC y^{-1} respectively). The larger range ~~magnitude~~ of IAV ~~derived~~ from ~~the GCL (~0.037 PgC y^{-1}) is similar to that of the prior and of the surface ocean pCO_2–based estimates but larger than those of the GOBMs (~0.019 PgC y^{-1}). The largest IAV estimates (mean value of 0.059±0.024 PgC y^{-1}) are associated with the~~ atmospheric inverse analyses~~ions, and~~ is influenced especially by high magnitude IAV estimates from the CarbonTracker ~~analyses~~ (~~e.g., CTE and~~ CT) inverse analysis. ~~indicate larger IAV magnitudes for this period of ~0.08 PgC y^{-1}).~~ Potential causes of the differences

Formatted: English (United Kingdom)
Formatted: Justified
Formatted: Font: (Default) +Body (Times New Roman)
Formatted: Justified
Formatted: Font: (Default) +Body (Times New Roman), 10 pt
Formatted: Font: (Default) +Body (Times New Roman)

among atmospheric inversion between the GCL and CAMS IAV estimates and those of the CarbonTracker estimates are the different prior ocean fluxes employed by the ~~different~~ inverse analyses, and the relative weighting assigned to the influence of atmospheric CO_2 observations (Jacobson et al., 2019). The GCL and CAMS estimates use the prior flux of Landschützer et al. (2016). CTE uses the prior flux or Rodenbeck et al. (2014) and the CarbonTracker inversions use the prior flux of Jacobson et al. (2007).

Recent synthesis studies of global ocean carbon fluxes have noted that GOBMs underestimate the magnitude of IAV in comparison to estimates from pCO_2–based mappings and inverse analyses (DeVries et al. 2019, Hauck et al. 2020). An important driver of IAV is the variability in biological carbon export; the lower variability observed in the GOBMs could result from opposing changes in biological vs. circulation impacts on carbon export, which potentially reduces the sensitivity of the GOBM air–sea carbon fluxes to climate variability (Landschutzer et al., 2013, DeVries et al., 2019).

~~The GCL estimate of IAV for the North Atlantic subpolar region (~0.025 PgC y^{-1}) is closer in magnitude to the majority of other analyses, which range between 0.015 and 0.036 PgC y^{-1} (the exception being the CT inverse estimate with the largest IAV of 0.114 PgC y^{-1}). For this region the IAV estimates from atmospheric inverse analyses display the greatest variation, influenced by the high estimate from the CT analysis.~~

Table 3. ~~.~~ Summary metrics of GEOSChem–LETKF North Atlantic (NA) CO_2 flux estimates, and comparison with independent estimates (from atmospheric inverse analyses, surface pCO_2 mappings, and Global Ocean Biogeochemistry models (GOBMs)) for the period 2000–2017. Listed are estimates for the interannual variability~~trend~~ of the regional fluxes over the period. The metrics listed in this table are plotted in Fig. 3 c, d.~~.~~

Interannual Variability (IAV) (PgC y^{-1})		
NA Subtropics (15°N–50°N)	**NA Subpolar** (50°N–80°N; eastern boundary at 20°E)	
Atmospheric inversions		
0.036±0.006	*0.034±0.009*	*This study (GCL)*[a]
0.032	0.023	CAMS (Chevallier et al. 2019)

Formatted: Font: (Default) +Body (Times New Roman)

Formatted: Font: (Default) +Body (Times New Roman), 10 pt

Formatted: Font: (Default) +Body (Times New Roman)

Formatted Table

0.065	0.064	CTE (van der Laan–Luijkx et al. 2017)
0.084	0.114	CT (Jacobson et al. 2020)
[0.032, 0.084]	[0.023, 0.114]	Range of all atmospheric inverse studies (minimum to maximum)
Surface ocean pCO_2–based flux products		
0.038	0.036	pCO_2La (Landschutzer et al. 2016)
0.050	0.035	pCO_2Ro (Rodenbeck et al. 2014)
0.031	0.018	CMEMS (Chau et al. 2020)
0.035	0.019	CSIR (Gregor et al. 2019)
0.028	0.009	JMA (Iida et al. 2015)
0.037	0.016	LSCEFFNN (Denvil–Sommer et al. 2019)
0.029	0.019	NIES (Zeng et al. 2015)
0.037	0.037	Watson et al. (2020)
[0.029, 0.050]	[0.009, 0.037]	Range of all pCO_2–based representations (minimum to maximum)
Global ocean biogeochemistry models		
0.018	0.018	NEMO–PlankTOM5 (Buitenhuis et al. 2010)
0.014	0.015	CCSM-BEC (Doney et al. 2009)
0.027	0.024	NEMO-PISCES (CNRM) (Séférian et al. 2013)
0.016	0.019	MPIOM-HAMOCC (Ilyina et al. 2013)
0.021	0.016	NorESM-OC (Schwinger et al. 2016)
0.017	0.016	MITgcm-REcoM2 (Hauck et al. 2016)
[0.014, 0.027]	[0.015, 0.024]	Range of GOBM studies (minimum to maximum)

[a] The uncertainty of the estimated IAV from the GCL (this study) is calculated as the standard deviation of the ensemble posterior fluxes.

Formatted: Font: (Default) +Body (Times New Roman), 10 pt

~~Interannual Variability (IAV) ($PgC\ y^{-1}$)~~		
~~NA Subtropics~~	~~NA Subpolar~~	
~~**Atmospheric inversions**~~		
~~*0.037±0.006*~~	~~*0.025±0.009*~~	~~*This study (GCL)*[c]~~
~~0.032~~	~~0.023~~	~~CAMS (Chevallier et al. 2019)~~
~~0.082~~	~~0.033~~	~~CTE (van der Laan–Luijkx et al. 2017)~~
~~0.084~~	~~0.114~~	~~CT (Jacobson et al. 2020)~~
~~0.059±0.024~~	~~0.049±0.038~~	~~Mean of all Atmospheric inverse studies~~[b]

Surface ocean pCO_2–based flux products		
0.038	0.036	pCO_2La (Landschutzer et al. 2016)
0.050	0.035	pCO_2Ro (Rodenbeck et al. 2013)
0.044±0.006	0.036±0.001	Mean of all pCO_2-based representations[b]
Global ocean biogeochemistry models		
0.018	0.018	NEMO–PlankTOM5 (Buitenhuis et al. 2010)
0.014	0.015	CCSM-BEC (Doney et al. 2009)
0.027	0.024	NEMO-PISCES (CNRM) (Séférian et al. 2013)
0.016	0.019	MPIOM-HAMOCC (Ilyina et al. 2013)
0.021	0.016	NorESM-OC (Schwinger et al. 2016)
0.017	0.016	MITgcm-REcoM2 (Hauck et al. 2016)
0.019±0.004	0.018±0.003	Mean of GOBM studies[b]

3.2.3 Estimated Trends of North Atlantic CO_2 Fluxes

Our calculations of estimated trends for the 2000–2017 period are presented in Table 4 and Fig. 3e and 3f. We also highlight in the table and figure panels, the trend estimates that are statistically significant Our GCL analyses indicate a statistically significant trend of -0.062±0.009 PgC y^{-1} $decade^{-1}$, i.e., increasing CO_2 uptake in the North Atlantic subtropical basin for the 2000–2017 period (significant at the 95% confidence level, with Ordinary Least Squares (OLS, Montgomery et al., 2012) method). Our GCL analyses indicate statistically significant trends for the 2000–2017 period of -0.064±0.007 PgC y^{-1} $decade^{-1}$ in the North Atlantic subtropical basin, and 0.063±0.008 PgC y^{-1} $decade^{-1}$ in the subpolar region. These estimated trends is are of larger similar magnitude to than those estimated from surface ocean pCO_2 products, but of much larger magnitude (by a factor of 3–4) than decadal trends estimated from the GOBMs air-sea fluxes (Fig. 3e, Table 4). Our findings are similar to those of Devries et al. (2019), who noted that decadal trend estimates of North Atlantic CO_2 uptake for the 2000s from the SOCOM inter–comparison of pCO_2–based flux products were larger than those from the GOBMS in their analysis (see Fig. 3 of their study). , and of similar magnitude to the trends derived for the surface ocean pCO_2–based estimates.

In the North Atlantic subpolar region, GCL estimate of the trend in regional CO_2 uptake of -0.026±0.015 PgC y^{-1} $decade^{-1}$ is larger than the mean estimate from GOBM analyses, and similar to the majority of other atmospheric inverse analyses (apart from the CT inversion which displays a large estimated trend of -0.1 PgC y^{-1} $decade^{-1}$). However, we also note that our derived estimate of trend for this region is not significant at the 95% confidence level.

Formatted: Font: (Default) +Body (Times New Roman)

Formatted: Font: (Default) +Body (Times New Roman)

Table 4. Summary metrics of GEOSChem–LETKF North Atlantic (NA) CO_2 flux estimates, and comparison with independent estimates (from atmospheric inverse analyses, surface pCO_2 mappings, and Global Ocean Biogeochemistry models (GOBMs)) for the period 2000–2017. Listed are estimates for the trend of the regional fluxes over the period. The metrics listed in this table are plotted in Fig. 3 e, f of the main study.

Trend (PgC y^{-1} $decade^{-1}$)		
NA Subtropics (15°N–50°N)	**NA Subpolar** (50°N–80°N; eastern boundary at 20°E)	
Atmospheric inversions		
-0.064±0.007 (S)[a]	*-0.063±0.008(S)*[a]	*This study (GCL)*[b]
-0.016	-0.023	CAMS (Chevallier et al. 2019)
-0.068	-0.028	CTE (van der Laan–Luijkx et al. 2017)
-0.067	-0.102	CT (Jacobson et al. 2020)
[-0.016, -0.085]	[-0.023, -0.126]	Range of all Atmospheric inverse studies (minimum to maximum)
Surface ocean pCO_2-based flux products		
-0.068(S)	-0.056(S)	pCO_2La (Landschutzer et al. 2016)
-0.070(S)	-0.029	pCO_2Ro (Rodenbeck et al. 2014)

Formatted: Space After: 0 pt

Formatted: Font: (Default) +Body (Times New Roman)

-0.057(S)	-0.027(S)	CMEMS (Chau et al. 2020)
-0.063(S)	-0.034(S)	CSIR (Gregor et al. 2019)
-0.048(S)	-0.001	JMA (Iida et al. 2015)
-0.070(S)	-0.021	LSCEFFNN (Denvil–Sommer et al. 2019)
-0.057(S)	-0.037(S)	NIES (Zeng et al. 2015)
-0.069(S)	-0.064(S)	Watson et al. (2020)
[-0.048, -0.070]	[-0.001,-0.064]	Range of all pCO_2–based representations (minimum to maximum)
Global ocean biogeochemistry models		
-0.015	-0.023	NEMO–PlankTOM5 (Buitenhuis et al. 2010)
-0.010	0.0002	CCSM–BEC (Doney et al. 2009)
-0.021	-0.002	NEMO–PISCES (CNRM) (Séférian et al. 2013)
-0.014	-0.011	MPIOM–HAMOCC (Ilyina et al. 2013)
-0.036(S)	-0.023	NorESM–OC (Schwinger et al. 2016)
-0.013	-0.014	MITgcm–REcoM2 (Hauck et al. 2016)
[-0.010, -0.036]	[-0.0002, -0.023]	Range of GOBM studies (minimum to maximum)

Trend (PgC y^{-1} $decade^{-1}$)		
NA Subtropics	NA Subpolar	
Atmospheric inversions		
-0.062±0.009 (S[d])	*-0.026±0.015*	*This study (GCL)[e]*
-0.016	-0.023	CAMS (Chevallier et al. 2019)
0.010	0.015	CTE (van der Laan–Luijkx et al. 2017)
-0.067	-0.102	CT (Jacobson et al. 2020)
-0.034±0.032	-0.041±0.035	Mean of all Atmospheric inverse studies[b]
Surface ocean pCO_2-based flux products		
-0.068	-0.056	pCO_2La (Landschutzer et al. 2016)
-0.070	-0.029	pCO_2Ro (Rodenbeck et al. 2013)
-0.069±0.001	-0.043±0.013	Mean of all pCO_2-based representations[b]
Global ocean biogeochemistry models		
-0.015	-0.023	NEMO-PlankTOM5 (Buitenhuis et al. 2010)
-0.010	0.000	CCSM-BEC (Doney et al. 2009)

~~-0.021~~	~~-0.002~~	~~NEMO-PISCES (CNRM) (Séférian et al. 2013)~~
~~-0.014~~	~~-0.011~~	~~MPIOM-HAMOCC (Ilyina et al. 2013)~~
~~-0.036~~	~~-0.023~~	~~NorESM-OC (Schwinger et al. 2016)~~
~~-0.013~~	~~-0.014~~	~~MITgcm-REcoM2 (Hauck et al. 2016)~~
~~-0.018±0.009~~	~~-0.018±0.009~~	~~Mean of GOBM studies[b]~~

~~[a] The uncertainty of long term mean estimate from the GCL (this study) is calculated as the standard deviation of the annual flux estimates over the (2000–2017) period.~~

~~[b] The uncertainty of atmospheric-inverse-based mean, pCO_2-based mean and GOBM-based mean is calculated as the standard deviation of products for each method.~~

~~[c] The uncertainty of the estimated IAV from the GCL (this study) is calculated as the standard deviation of the ensemble posterior fluxes~~

[d]a The symbol (S) indicates that the calculated trend is statistically significant (at the 95% confidence interval).

[e]b The uncertainty of the fitted trend from the GCL estimates is reported as 1 standard deviation of the OLS fitted slope (Montgomery et al. 2012).

Formatted: Font: 9 pt

4 Summary

In this study we present a new long term estimate of North Atlantic air–sea CO_2 fluxes for recent decades (period 2000–2017) using the atmospheric carbon cycle data assimilation system GEOSChem–LETKF. We focus, in particular, on the specification of prior ocean fluxes, including sensitivity of flux estimates to alternative prior flux distributions, and on the specification of uncertainties associated with ocean fluxes. Towards this we have developed the 'spread-based' flux uncertainty scheme which represents the variability among a set of different prior ocean CO_2 flux representations. The scheme ascribes higher levels of uncertainty to regions with larger discrepancies among ocean CO_2 prior flux representation that arise from uncertainties associated with measurement density and pCO_2–interpolation methods (Sect. 2.4). The spread-based flux uncertainty scheme provides improved performance in comparison to schemes with fixed prior flux uncertainty levels, based on an assessment metric of differences in model–observation values for atmospheric CO_2 at North Atlantic measurement sites of the NOAA–GLOBALVIEWCO_2 network (Sect. 3.1). It provides a valuable new means of specifying prior flux uncertainties for atmospheric inverse analyses of ocean CO_2 fluxes.

Formatted: English (United Kingdom)

We have used the spread–based flux uncertainty scheme in the GEOSChem–LETKF to derive ~~Our GCL~~ estimates of CO_2 ~~uptake~~ fluxes in the North Atlantic for the 2000–2017 period. Long term mean estimates of the regional ocean CO_2 uptake are -0.~~26~~255±0.~~04~~ 037 PgC y^{-1} for the North Atlantic subtropics and -0.~~25~~203±0.~~04~~ 037 PgC y^{-1} for North Atlantic subpolar region., and are consistent with recent regional flux estimates from surface pCO_2–based methods and global ocean biogeochemistry models (GOBMs). The GEOSChem–LETKF ~~GCL~~ estimates of interannual variability in air–sea CO_2 fluxes

are 0.037036±0.006 PgC y^{-1} (North Atlantic subtropics) and 0.025034±0.009 PgC y^{-1} (North Atlantic subpolar). In common with estimates from other atmospheric CO_2 inverse studies, the magnitude of IAV derived from the GEOSChem–LETKF is larger than corresponding estimates from GOBMs. Our GEOSChem–LETKF CL estimates also indicate a statistically significant trends of increasing CO_2 uptake for the North Atlantic subtropicals and subpolar region (estimated trend of -0.062064±0.009 007 and -0.063±0.008 PgC y^{-1} $decade^{-1}$ respectively). These trends are of comparable magnitude to those estimated from surface pCO_2–based flux products, but much larger than those derived from global ocean biogeochemistry models for the 2000-2017 period.

Our GCL estimates of long term mean CO_2 uptake for the 2000–2017 period for both NA subtropics and subpolar regions lie between the estimates from other inverse analyses (e.g., Chevallier et al., 2019 (lower) and the CarbonTracker derived analyses of Jacobson et al., 2020 (higher)); primary causes are the different prior flux representations used in the CarbonTracker analyses. Our GCL estimates of long term North Atlantic CO_2 uptake are similar in magnitude to long term ensemble mean estimates from surface–ocean pCO_2 methods and GOBMs (Fig. 3). The magnitude of IAV derived from the GCL is similar to that of the surface ocean pCO_2–based estimates but larger than those of the GOBMs for both NA regions. In this study we have also evaluated a comparison of alternative specifications of the prior flux uncertainty (section 3.2), and present long term flux estimates derived using a spread–based flux uncertainty scheme. This scheme enables representation of the variability among alternative prior ocean CO_2 flux representations and ascribes higher levels of uncertainty to regions with larger discrepancies among prior flux representations; it is therefore preferable to the fixed prior flux uncertainty levels commonly used in inverse analyses. Incorporation of additional prior flux representations of ocean CO_2 (e.g., Roedenbeck et al., 2015) will improve the contribution of this scheme.

Air–sea CO_2 flux eEstimates of inter–annual variability and long term trends and associated metrics derived from our GEOSChem–LETKF GCL analyses are generally more robust for the North Atlantic subtropics than for the NA subpolar region, and characterized by smaller uncertainty bounds. Limiting factors affecting estimates for the North Atlantic subpolar region include higher levels of uncertainty associated with (a) specification of prior fluxes (Fig. 1), and (b) the observational uncertainty at the atmospheric measurement CO_2 sites in these high northern latitudes (Table A1). The number of regional atmospheric CO_2 measurement sites available to constrain North Atlantic subpolar fluxes are also relatively few in comparison to the subtropical region. Improved ocean CO_2 flux estimates and associated metrics for this North Atlantic region will be obtained by provision of additional high accuracy marine boundary layer CO_2 measurements for the region from fixed surface sites and from ships and buoys (Wanninkhof et al., 2019).

Appendix A: The Local Ensemble Transform Kalman Filter (LETKF) system

Here we briefly describe the LETKF system used for estimation of surface CO_2 fluxes. The methodology follows that of Hunt et al. (2007) and Miyoshi et al. (2007), and additional detail is provided in these publications. The LETKF has been previously used in meteorological forecasting, and more recently in atmospheric CO_2 data assimilation (e.g., Liu et al. 2019, 2016; Kang et al. 2012). The LETKF provides iterative estimates of the time evolution of the system state, *x,* (here representing the gridscale surface carbon fluxes, of dimension *m*). Each step involves a forecast stage (based on a physical model of the system evolution) and a state estimation stage (the 'analysis' step), which combines system observations, *y* (of dimension *n*), together with the background forecast, x^b, to derive the improved state estimate. The observation operator *H* provides the mapping from the state space to the observation space; in this study *H* is provided by the GEOSChem atmospheric model. In the analysis step, the surface carbon flux estimates are obtained by minimization of a cost function (~~Equation~~ Eq. ~~S1~~A1) which accounts for deviations of the system state *x*, from the background forecast, x^b, and for the mismatch between observations (*y*) and their modeled representations (*Hx*) :

$$J(x) = (x - x^b)^T P\mathit{B}^{-1}(x - x^b) + (y - Hx)^T R^{-1}(y - Hx) \quad \text{(A1)}$$

B represents the background flux covariance matrix, and *R* represents the observation covariance matrix.

In the LETKF system, an ensemble of model simulations is used to calculate the sample mean and covariance of the system state; thus, the background state x^b is given by $(x^{b(i)}: i = 1.2, \dots k)$ for k ensemble members. The sample mean $\bar{x}^b$ and covariance P^b of the background state vector given by :

$$\bar{x}^b = k^{-1} \sum_{i=1}^{k} x^{b(i)} \quad \text{(A2)}$$

$$P^b = (k-1)^{-1} \sum_{i=1}^{k} \left(x^{b(i)} - \bar{x}^b\right)\left(x^{b(i)} - \bar{x}^b\right)^T \quad \text{(A3)}$$

$$= (k-1)^{-1} X^b (X^b)^T$$

X^b is an *m*×*k* matrix whose *i*th column is $x^{b(i)} - \bar{x}^b$. P^b is the background state covariance matrix (*m*×*m*).

Similarly the analysis state is represented by the ensemble $(x^{a(i)}: i = 1,2, \dots k)$ with its sample mean and covariance given by:

$$\bar{x}^a = k^{-1} \sum_{i=1}^{k} x^{a(i)} \quad \text{(A4)}$$

$$P^a = (k-1)^{-1} \sum_{i=1}^{k} \left(x^{a(i)} - \bar{x}^a\right)\left(x^{a(i)} - \bar{x}^a\right)^T \quad \text{(A5)}$$

$$= (k-1)^{-1} X^a (X^a)^T$$

where X^a is the *m*×*k* matrix whose ith column is $x^{a(i)} - \bar{x}^a$.

The analysis state and covariance $\bar{x}^a$ and P^a are updated based on the background information $\bar{x}^b$ and observations y through the following equations:

$$\bar{x}^a = \bar{x}^b + P^a H^T R^{-1}(y - Hx^b) \quad \text{(A6)}$$

$$P^a = (I + P^b H^T R^{-1} H)^{-1} P^b \quad \text{(A7)}$$

The ensemble $y^{b(i)}$ of background observation vectors is defined by:

$$y^{b(i)} = H(x^{b(i)}) \quad \text{(A8)}$$

$$H(\bar{x}^b + X^b w) \approx \bar{y}^b + Y^b w \quad \text{(A9)}$$

where Y^b is the $n \times k$ matrix whose ith column is $(y^{b(i)} - \bar{y}^b)$, and w is a Gaussian random vector with mean $\bar{w}^b = 0$ and covariance $\tilde{P}^b = (k-1)^{-1} I$ .Then the analogues of analysis equations (6) and (7) are:

$$\bar{w}^a = \tilde{P}^a (Y^b)^T R^{-1}(y - \bar{y}^b) \quad \text{(A10)}$$

$$\tilde{P}^a = [(k-1)I + (Y^b)^T R^{-1} Y^b]^{-1} \quad \text{(A11)}$$

Following Hunt et al. (2007) and Miyoshi et al. (2007) (refer to these publications for the complete LETKF derivation) the overall analysis equation is:

$$x = \bar{x}^b + X^b [\tilde{P}^a (Y^b)^T R^{-1}(y - \bar{y}^b) + [(k-1)\tilde{P}^a]^{1/2}] \quad \text{(A12)}$$

The LETKF allows flexibility in the choice of observations to be assimilated at each grid point, based on the distance (r) of the observations from the gridpoint. The localization weighting function $f(r)$ is given by:

$$f(r) = \exp\left(-\frac{r^2}{2L^2}\right) \quad \text{(A13)}$$

where L is an observation localization length which can be predefined to determine the outer boundary of the influence of the observations; i.e., the localization weighting function drops to zero at a value of

$$r = 2.\sqrt{\frac{10}{3}} L \quad \text{(A14)}$$

The observation localization is realized by multiplying the inverse of the localization function $f(r)$ with the observational error covariance R.

The parameter L represents the horizontal localization radius, and is set to 2000 km for this study, following Liu et al. (2016). The localization radius is used in the LETKF in a latitude–dependent weighting function which characterizes the spatial scale of the region within which atmospheric CO_2 observations are assimilated at each gridpoint (Miyoshi et al. 2007).

620

Table A1. Atmospheric CO_2 measurement sites[a]

Site code	Longitude (degrees)	Latitude (degrees)	Altitude (m)	Site name	U[b] (ppm)
ABP	-38.16	-12.76	6	Arembepe, Bahia	1.04
ALT	-62.51	82.45	195	Alert, Nunavut	1.34
AMY	126.33	36.54	125	Anmyeon-do	8.88
ASC	-14.40	-7.97	90	Ascension Island	0.66
ASK	5.63	23.26	2715	Assekrem	0.80
AZR	-27.08	38.75	24	Terceira Island, Azores	2.26
BAL	16.67	55.50	28	Baltic Sea	5.50
BCS	-110.20	23.30	14	Baja California Sur	3.42
BGU	3.23	41.97	13	Begur	3.93
BHD	174.87	-41.41	90	Baring Head Station	1.12
BKT	100.32	-0.20	875	Bukit Kototabang	3.49
BME	-64.65	32.37	17	St. Davids Head, Bermuda	2.57
BMW	-64.88	32.27	60	Tudor Hill, Bermuda	2.12
BRW	-156.60	71.32	28	Barrow Atmospheric Baseline Observatory	1.88
BSC	28.67	44.18	5	Black Sea, Constanta	9.88
CBA	-162.72	55.20	25	Cold Bay, Alaska	2.41
CFA	147.06	-19.28	5	Cape Ferguson, Queensland	1.04
CGO	144.68	-40.68	164	Cape Grim, Tasmania	0.40
CHR	-157.15	1.70	5	Christmas Island	0.60
CIB	-4.93	41.81	850	Centro de Investigacion de la Baja Atmosfera (CIBA)	3.97
CPT	18.49	-34.35	260	Cape Point	0.74
CRI	73.83	15.08	66	Cape Rama	3.47
CRZ	51.85	-46.43	202	Crozet Island	0.49
CYA	110.52	-66.28	55	Casey, Antarctica	0.29
DRP	-64.91	-55.00	10	Drake Passage	0.41
DSI	116.73	20.70	8	Dongsha Island	3.46

EIC	-109.45	-27.15	55	Easter Island	1.80
ELL	0.96	42.58	2005	Estany Llong	2.41
ESP	-126.53	49.38	47	Estevan Point, British Columbia	1.49
FKL	25.67	35.34	150	Finokalia, Crete	3.34
GMI	144.66	13.39	6	Mariana Islands	2.22
GPA	131.05	-12.25	37	Gunn Point	2.02
HBA	-26.21	-75.61	35	Halley Station, Antarctica	0.16
HPB	11.02	47.80	990	Hohenpeissenberg	6.71
HSU	-124.73	41.05	8	Humboldt State University	5.78
HUN	16.65	46.95	344	Hegyhatsal	6.00
ICE	-20.29	63.40	127	Storhofdi, Vestmannaeyjar	2.03
IZO	-16.48	28.30	2378	Izana, Tenerife, Canary Islands	1.21
KEY	-80.20	25.67	6	Key Biscayne, Florida	4.14
KUM	-154.82	19.52	8	Cape Kumukahi, Hawaii	1.77
KZD	75.57	44.45	412	Sary Taukum	3.19
KZM	77.88	43.25	2524	Plateau Assy	3.00
LJO	-117.26	32.87	20	La Jolla, California	2.72
LLB	-112.45	54.95	546	Lac La Biche, Alberta	8.91
LLN	120.86	23.46	2867	Lulin	5.27
LMP	12.61	35.51	50	Lampedusa	2.08
MAA	62.87	-67.62	42	Mawson Station, Antarctica	0.32
MEX	-97.31	18.98	4469	High Altitude Global Climate Observation Center	1.33
MHD	-9.90	53.33	26	Mace Head, County Galway	3.23
MID	-177.37	28.22	8	Sand Island, Midway	1.39
MKN	37.30	-0.06	3649	Mt. Kenya	1.98
MLO	-155.58	19.53	3402	Mauna Loa, Hawaii	0.63
MQA	158.97	-54.48	13	Macquarie Island	0.33
NAT	-35.26	-5.52	20	Farol De Mae Luiza Lighthouse	1.44
NMB	15.03	-23.58	461	Gobabeb	1.13
NWR	-105.58	40.05	3526	Niwot Ridge, Colorado	1.88
OBN	36.60	55.12	484	Obninsk	6.49
OTA	142.82	-38.52	50	Otway, Victoria	17.45
OXK	11.81	50.03	1185	Ochsenkopf	8.18

PAL	24.12	67.97	570	Pallas-Sammaltunturi, GAW Station	3.72
PDM	0.14	42.94	2877	Pic Du Midi	2.71
POC	-145.13	14.97	20	Pacific Ocean	1.47
PSA	-64.00	-64.92	15	Palmer Station, Antarctica	0.23
PTA	-123.73	38.95	22	Point Arena, California	5.50
RK1	-177.90	-29.20	12	Kermadec Island	2.23
RPB	-59.43	13.17	20	Ragged Point	0.83
SDZ	117.12	40.65	298	Shangdianzi	9.57
SEY	55.53	-4.68	7	Mahe Island, Seychelles	0.98
SGP	-97.48	36.62	374	Southern Great Plains, Oklahoma	4.91
SHM	174.10	52.72	28	Shemya Island, Alaska	2.91
SIS	-1.26	60.09	33	Shetland Islands	2.87
SMO	-170.57	-14.25	47	Tutuila, American Samoa	1.19
STM	2.00	66.00	7	Ocean Station M	2.03
SUM	-38.42	72.60	3215	Summit	1.32
SYO	39.58	-69.00	16	Syowa Station, Antarctica	0.23
TAC	1.14	52.52	236	Tacolneston	6.78
TAP	126.13	36.73	21	Tae-ahn Peninsula	6.90
THD	-124.15	41.05	112	Trinidad Head, California	4.54
TIK	128.89	71.60	29	Hydrometeorological Observatory of Tiksi	2.64
USH	-68.31	-54.85	32	Ushuaia	1.41
UTA	-113.72	39.90	1332	Wendover, Utah	2.65
UUM	111.10	44.45	1012	Ulaan Uul	2.78
WIS	34.78	30.86	482	Weizmann Institute of Science at the Arava Institute, Ketura	2.39
WLG	100.92	36.27	3815	Mt. Waliguan	2.26
WPC	167.50	-29.86	10	Western Pacific Cruise	1.70
ZEP	11.89	78.91	479	Ny-Alesund, Svalbard	1.82

[a] Source reference: Cooperative Global Atmospheric Data Integration Project, 2018. Version: obspack_co2_1_GLOBALVIEWplus_v4.2_2019-03-19 (https://doi.org/10.25925/20190319)

[b] The specification of observational uncertainty U on atmospheric CO_2 measurements (and represented in matrix *R* of ~~Equation~~ Eq. A1) is calculated as the standard deviation of measurement variability and using the detrended and deseasonalized CO_2 time series at each measurement site (following methods of Chevallier et al. ~~(~~2010)~~)~~.

Table A2: Model–Observation mismatch in atmospheric CO_2 concentrations (unit: ppm) at North Atlantic sites (average over year 2003). GCL model values are derived from the a posteriori model analyses associated with the sensitivity analyses of Sect. 3.1. Atmospheric CO_2 observations are from the NOAA–GLOBALVIEW network described in Sect. 2.3.

Sensitivity Analyses (Sect. 2.3)	North Atlantic Sites						Global Network Average
	BMW	KEY	AVI	AZR	IZO	ICE	
U1Ta	0.81	0.88	0.76	1.49	1.83	1.20	0.54
U2Ta	0.71	0.82	0.69	1.42	1.74	1.13	0.44
U3Ta	0.58	-0.20	0.36	0.85	1.64	0.40	0.01
U1La	0.92	0.93	0.76	1.60	1.94	1.44	0.61
U2La	0.84	0.87	0.68	1.53	1.86	1.38	0.51
U3La	0.52	-0.27	0.21	0.84	1.58	0.58	0.04
U1Ro	0.74	0.74	0.54	1.35	1.66	0.98	0.35
U2Ro	0.66	0.68	0.47	1.28	1.57	0.91	0.26
U3Ro	0.55	-0.28	0.21	0.73	1.48	0.27	-0.11

Data Availability.

Data sources: (i) Atmospheric CO_2 measurements were taken from obspack_co2_1_GLOBALVIEWplus_v4.2_2019-03-19 (https://doi.org/10.25925/20190319); (ii) Prior ocean flux oc_v1.7 from Rödenbeck et al . (2013) taken from http://www.bgc-jena.mpg.de/CarboScope/. Prior ocean flux Landschützer et al. (2016) taken from https://www.nodc.noaa.gov/ocads/oceans/SPCO2_1982_present_ETH_SOM_FFN.html. Prior ocean flux from Takahashi et al. (2009) taken from ftp://ftp.as.harvard.edu/gcgrid/geos-chem. (iii) CarbonTracker CT2019 results provided by NOAA ESRL, Boulder, Colorado, USA from the website at http://carbontracker.noaa.gov. CTE flux estimates taken from ftp://ftp.wur.nl/carbontracker/data/fluxes/data_flux1x1_monthly/ **on 24 November 2020**. The flux estimates from CAMS(v18r2) taken from https://apps.ecmwf.int/datasets/data/cams-ghg-inversions/. (iv) The model CO_2 fluxes for JULES (land) and GOBMs (ocean) taken from (Le Quéré et al., 2018). Time series of reconstructed surface ocean pCO_2 and CO_2 fluxes (LSCEFFNN) from Denvil–Sommer et al., 2019 are the first version of CMEMS, downloaded from http://marine.copernicus.eu/services-portfolio/access-to-products/. The products from Iida et al., 2015 downloaded from http://www.data.jma.go.jp/gmd/kaiyou/english/co2_flux/co2_flux_data_en.html. The products from Zeng et al., 2015

Formatted: Justified
Formatted: Font: 9 pt
Formatted: Font: 9 pt
Formatted: Space Before: 0 pt, After: 0 pt, Line spacing: 1.5 lines
Field Code Changed
Field Code Changed
Field Code Changed
Field Code Changed
Field Code Changed
Formatted: Font: Bold
Field Code Changed

downloaded from https://db.cger.nies.go.jp/DL/10.17595/20201020.001.html.en. The products from CMEMS, CSIR, Watson taken from Friedlingstein et al., 2020.

Formatted: Font: Bold, Not Italic, Font color: Black

Formatted: Normal, Left, Space Before: 0 pt, After: 0 pt

Author contributions. ZC and PS designed the study. ZC, PS, JZ and NZ developed the model. ZC, PS, AW, and US discussed the design of simulations. ZC performed the simulations and analysis and wrote the initial manuscript. All authors contributed to the writing of the paper.

Competing interests. The authors declare that they have no conflict of interest.

Disclaimer. The work reflects only the author's view,the Europen Commission and their executive agency are not responsible for any use that may be made of the information the work contains.

Acknowledgements. This work was performed using the High Performance Computing Cluster at the University of East Anglia.

Financial support. It was supported through the UK Natural Environment Research Council grants NE/K002473/1(RAGNARoCC).

References

Bakker, D. C. E., Pfeil, B., Landa, C. S., Metzl, N., O'Brien, K. M., Olsen, A., Smith, K., Cosca, C., Harasawa, S., Jones, S. D., Nakaoka, S., Nojiri, Y., Schuster, U., Steinhoff, T., Sweeney, C.,Takahashi, T., Tilbrook, B., Wada, C., Wanninkhof, R., Alin, S. R., Balestrini, C. F., Barbero, L., Bates, N. R., Bianchi, A. A., Bonou, F., Boutin, J., Bozec, Y., Burger, E. F., Cai, W.-J., Castle, R. D., Chen, L., Chierici, M., Currie, K., Evans, W., Featherstone, C., Feely, R. A., Fransson, A., Goyet, C., Greenwood, N.,Gregor, L., Hankin, S., Hardman-Mountford, N. J., Harlay, J., Hauck, J., Hoppema, M., Humphreys, M. P., Hunt, C. W., Huss, B., Ibánhez, J. S. P., Johannessen, T., Keeling, R., Kitidis, V., Körtzinger, A., Kozyr, A., Krasakopoulou, E., Kuwata, A., Landschützer, P., Lauvset, S. K., Lefèvre, N., Lo Monaco, C., Manke, A., Mathis, J. T., Merlivat, L., Millero, F. J., Monteiro, P. M. S., Munro, D. R., Murata, A., Newberger, T., Omar, A. M., Ono, T., Paterson, K., Pearce, D., Pierrot, D., Robbins, L. L., Saito, S., Salisbury, J., Schlitzer, R., Schneider, B., Schweitzer, R., Sieger, R., Skjelvan, I., Sullivan, K. F., Sutherland, S. C., Sutton, A. J., Tadokoro, K., Telszewski, M., Tuma, M., van Heuven, S. M. A. C., Vandemark, D., Ward, B., Watson, A. J., and Xu, S.: A multidecade record of high-quality fCO2 data in version 3 of the Surface Ocean CO_2 Atlas (SOCAT), Earth Syst. Sci. Data, 8, 383–413, https://doi.org/10.5194/essd-8-383-2016, 2016.

Formatted: Normal

Bopp, L., Resplandy, L., Orr, J. C., Doney, S. C., Dunne, J. P., Gehlen, M., Halloran, P., Heinze, C., Ilyina, T., and Seferian, R.: Multiple stressors of ocean ecosystems in the 21st century: projections with CMIP5 models, Biogeosciences, 10, 6225-6245, https://doi.org/10.5194/bg-10-6225-2013, 2013.

Buitenhuis, E. T., Rivkin, R. B., Sailley, S., and Le Quéré, C.: Biogeochemical fluxes through microzooplankton, Global Biogeochemical Cycles, 24, GB4015, https://doi.org/10.1029/2009GB003601, 2010.

Carouge, C., Bousquet, P., Peylin, P., Rayner, P., and Ciais, P.: What can we learn from European continuous atmospheric CO_2 measurements to quantify regional fluxes--Part 1: Potential of the 2001 network, Atmospheric Chemistry & Physics, 10, 3107-3117, https://doi.org/10.5194/acp-10-3107-2010, 2010.

Chatterjee, A., Engelen, R. J., Kawa, S. R., Sweeney, C., and Michalak, A. M.: Background error covariance estimation for atmospheric CO_2 data assimilation, Journal of Geophysical Research: Atmospheres, 118, 10140-10154, https://doi.org/10.1002/jgrd.50564, 2013.

Chau, T. T., Gehlen, M., and Chevallier, F.: Global Ocean Surface Carbon Product MULTIOBS_GLO_BIO_CARBON_SURFACE_REP_015_008, E.U. Copernicus Marine Service Information, available at: https://resources.marine.copernicus.eu/?option=com_cswandview=detailsandproduct_id=MULTIOBS_G, last access:16 November 2020.

Chevallier, F., Ciais, P., Conway, T., Aalto, T., Anderson, B., Bousquet, P., Brunke, E., Ciattaglia, L., Esaki, Y., and Fröhlich, M.: CO_2 surface fluxes at grid point scale estimated from a global 21 year reanalysis of atmospheric measurements, Journal of Geophysical Research: Atmospheres, 115, D21307, https://doi.org/10.1029/2010JD013887, 2010.

Chevallier, F., Palmer, P. I., Feng, L., Boesch, H., O'Dell, C. W., and Bousquet, P.: Toward robust and consistent regional CO_2 flux estimates from in situ and spaceborne measurements of atmospheric CO_2, Geophysical Research Letters, 41, 1065-1070, https://doi.org/10.1002/2013GL058772, 2014.

Chevallier, F., Remaud, M., O'Dell, C. W., Baker, D., Peylin, P., and Cozic, A.: Objective evaluation of surface-and satellite-driven carbon dioxide atmospheric inversions, Atmospheric Chemistry and Physics, 19, 14233-14251, https://doi.org/10.5194/acp-19-14233-2019, 2019.

Clark, D., Mercado, L., Sitch, S., Jones, C., Gedney, N., Best, M., Pryor, M., Rooney, G., Essery, R., Blyth, E., Boucher, O., Harding, R., Huntingford, C., and Cox, P.: The Joint UK Land Environment Simulator (JULES), model description - Part 2: Carbon fluxes and vegetation dynamics, Geoscientific Model Development, 4, 701-722, https://doi.org/10.5194/gmd-4-701-2011, 2011.

Crippa, M., Janssens-Maenhout, G., Dentener, F., Guizzardi, D., Sindelarova, K., Muntean, M., Van Dingenen, R., and Granier, C.: Forty years of improvements in European air quality: regional policy-industry interactions with global impacts, Atmospheric Chemistry and Physics, 16, 3825-3841, https://doi.org/10.5194/acp-16-3825-2016, 2016.

Denvil-Sommer, A., Gehlen, M., Vrac, M., and Mejia, C.: LSCEFFNN-v1: a two-step neural network model for the reconstruction of surface ocean pCO_2 over the global ocean, Geosci. Model Dev., 12, 2091–2105, https://doi.org/10.5194/gmd-12- 2091-2019, 2019.~~Deng, F., Jones, D. B. A., Parazoo, N. C., O'Dell, C. W., and Nassar, R.: Combining GOSAT XCO_2~~

observations over land and ocean to improve regional CO_2 flux estimates, Journal of Geophysical Research: Atmospheres, 121, 1896-1913, https://doi.org/10.1002/2015JD024157, 2016.

DeVries, T., Le Quéré, C., Andrews, O., Berthet, S., Hauck, J., Ilyina, T., Landschützer, P., Lenton, A., Lima, I. D., and Nowicki, M.: Decadal trends in the ocean carbon sink, Proceedings of the National Academy of Sciences, 116, 11646-11651, https://doi.org/10.1073/pnas.1900371116, 2019.

Doney, S. C., Lima, I., Feely, R. A., Glover, D. M., Lindsay, K., Mahowald, N., Moore, J. K., and Wanninkhof, R.: Mechanisms governing interannual variability in upper-ocean inorganic carbon system and air–sea CO_2 fluxes: Physical climate and atmospheric dust, Deep Sea Research Part II: Topical Studies in Oceanography, 56, 640-655, https://doi.org/10.1016/j.dsr2.2008.12.006, 2009.

Feng, L., Palmer, P., Bösch, H., and Dance, S.: Estimating surface CO_2 fluxes from space-borne CO_2 dry air mole fraction observations using an ensemble Kalman Filter, Atmospheric Chemistry & Physics, 9, 2619-2633, https://doi.org/10.5194/acp-9-2619-2009, 2009.

Feng, L., Palmer, P. I., Parker, R. J., Deutscher, N. M., Feist, D., Kivi, R., Morino, I., and Sussmann, R.: Estimates of European uptake of CO_2 inferred from GOSAT XCO_2 retrievals: sensitivity to measurement bias inside and outside Europe, Atmospheric Chemistry and Physics, 16, 1289-1302, https://doi.org/10.5194/acp-16-1289-2016, 2016.

Friedlingstein, P., O'Sullivan, M., Jones, M. W., Andrew, R. M., Hauck, J., Olsen, A., Peters, G. P., Peters, W., Pongratz, J., Sitch, S., Le Quéré, C., Canadell, J. G., Ciais, P., Jackson, R. B., Alin, S., Aragão, L. E. O. C., Arneth, A., Arora, V., Bates, N. R., Becker, M., Benoit-Cattin, A., Bittig, H. C., Bopp, L., Bultan, S., Chandra, N., Chevallier, F., Chini, L. P., Evans, W., Florentie, L., Forster, P. M., Gasser, T., Gehlen, M., Gilfillan, D., Gkritzalis, T., Gregor, L., Gruber, N., Harris, I., Hartung, k., Haverd, V., Houghton, R. A., Ilyina, T., Jain, A. K.,Joetzjer, E., Kadono, K., Kato, E., Kitidis, V., Korsbakken, J. I., Landschützer, P., Lefèvre, N., Lenton, A., Lienert, S., Liu, Z., Lombardozzi, D., Marland, G., Metzl, N., Munro, D. R., Nabel, J. E. M. S., Nakaoka, S., Niwa, Y., O'Brien, K., Ono, T., Palmer, P. I., Pierrot, D., Poulter, B., Resplandy, L., Robertson, E., Rödenbeck, C., Schwinger, J., Séférian, R., Skjelvan, I., Smith, A. J. P., Sutton, A. J., Tanhua, T., Tans, P. P., Tian, H., Tilbrook, B., van der Werf, G., Vuichard, N., Walker, A. P., Wanninkhof, R., Watson, A. J., Willis, D., Wiltshire, A. J., Yuan, W., Yue, X., and Zaehle, S.: Global carbon budget 2020. Earth System Science Data, 12, 3269-3340, https://doi.org/10.5194/essd-12-3269-2020, 2020.Friedlingstein, P., Jones, M. W., O'Sullivan, M., Andrew, R. M., Hauck, J., Peters, G. P., Peters, W., Pongratz, J., Sitch, S., Le Quéré, C., Bakker, D. C. E., Canadell, J. G., Ciais, P., Jackson, R. B., Anthoni, P., Barbero, L., Bastos, A., Bastrikov, V., Becker, M., Bopp, L., Buitenhuis, E., Chandra, N., Chevallier, F., Chini, L. P., Currie, K. I., Feely, R. A., Gehlen, M., Gilfillan, D., Gkritzalis, T., Goll, D. S., Gruber, N., Gutekunst, S., Harris, I., Haverd, V., Houghton, R. A., Hurtt, G., Ilyina, T., Jain, A. K., Joetzjer, E., Kaplan, J. O., Kato, E., Goldewijk, K. K., Korsbakken, J. I., Landschützer, P., Lauvset, S. K., Lefèvre, N., Lenton, A., Lienert, S., Lombardozzi, D., Marland, G., McGuire, P. C., Melton, J. R., Metzl, N., Munro, D. R., Nabel, J. E. M. S., Nakaoka, S. I., Neill, C., Omar, A. M., Ono, T., Peregon, A., Pierrot, D., Poulter, B., Rehder, G., Resplandy, L., Robertson, E., Rödenbeck, C., Séférian, R., Schwinger, J.,

~~Smith, N., Tans, P. P., Tian, H. Q., Tilbrook, B., Tubiello, F. N., van der Werf, G. R., Wiltshire, A. J., and Zaehle, S.: Global Carbon Budget 2019, Earth System Science Data, 11, 1783-1838, https://doi.org/10.5194/essd-11-1783-2019, 2019.~~

Gaubert, B., Stephens, B. B., Basu, S., Chevallier, F., Deng, F., Kort, E. A., Patra, P. K., Peters, W., Rödenbeck, C., and Saeki, T.: Global atmospheric CO_2 inverse models converging on neutral tropical land exchange, but disagreeing on fossil fuel and atmospheric growth rate, Biogeosciences, 16, 117-134, https://doi.org/10.5194/bg-16-117-2019, 2019.

Gregor, L., Lebehot A., Kok, S., Monteiro P.: A comparative assessment of the uncertainties of global surface ocean CO2 estimates using a machine-learning ensemble (CSIR-ML6 version 2019a) -have we hit the wall?. Geoscientific Model Development, 12, 5113–5136, https://doi.org/10.5194/gmd-12-5113-2019, 2019.

Gruber, N., Gloor, M., Mikaloff Fletcher, S. E., Doney, S. C., Dutkiewicz, S., Follows, M. J., Gerber, M., Jacobson, A. R., Joos, F., and Lindsay, K.: Oceanic sources, sinks, and transport of atmospheric CO_2, Global Biogeochemical Cycles, 23, GB1005, https://doi.org/10.1029/2008GB003349, 2009.

Gruber, N., Landschützer, P., and Lovenduski, N. S.: The variable Southern Ocean carbon sink, Annual Review of Marine Science, 11, 159-186, https://doi.org/10.1146/annurev-marine-121916-063407, 2019.

Gurney, K., Law, R., Denning, A. S., Rayner, P. J., Baker, D., Bousquet, *P.*, Bruhwiler, L., Chen, Y. H., Ciais, P., Fan, S., Fung, I. Y., Gloor, M., Heimann, M., Higuchi, K., John, J., Maki, T., Maksyutov, S., Masarie, K., Peylin, P., Prather, M., Pak, B.C., Randerson, J., Sarmiento, J., Taguchi, S., Takahashi, T., and Yuan, C.: Towards robust regional estimates of CO_2 sources and sinks using atmospheric transport models, Nature, 415, 626–630, https://doi.org/10.1038/415626a, 2002.

Gurney, K. R., Law, R. M., Denning, A. S., Rayner, P. J., Baker, D., Bousquet, P., Bruhwiler, L., Chen, Y. H., Ciais, P., and Fan, S.: TransCom 3 CO_2 inversion intercomparison: 1. Annual mean control results and sensitivity to transport and prior flux information, Tellus B: Chemical and Physical Meteorology, 55B, 555-579, https://doi.org/10.3402/tellusb.v55i2.16728, 2003.

Hauck, J., Köhler, P., Wolf-Gladrow, D., and Völker, C.: Iron fertilisation and century-scale effects of open ocean dissolution of olivine in a simulated CO_2 removal experiment, Environmental Research Letters, 11, 024007, https://doi.org/10.1088/1748-9326/11/2/024007, 2016.

Hauck, J., Zeising, M., Le Quéré, C., Gruber, N., Bakker, D. C., Bopp, L., Chau, T. T., Gürses, Ö., Ilyina, T., Landschützer, P., Lenton, A., Resplandy, L., Rödenbeck, C., Schwinger, J., and Séférian, R.: Consistency and challenges in the ocean carbon sink estimate for the Global Carbon Budget. Frontiers in Marine Science, 7, 852, https://doi.org/10.3389/fmars.2020.571720, 2020.

Hunt, B. R., Kostelich, E. J., and Szunyogh, I.: Efficient data assimilation for spatiotemporal chaos: A local ensemble transform Kalman filter, Physica D: Nonlinear Phenomena, 230, 112-126, https://doi.org/10.1016/j.physd.2006.11.008, 2007.

Iida, Y., Kojima, A., Takatani, Y., Nakano, T. Midorikawa, T., and Ishii, M.: Trends in pCO_2 and sea-air CO_2 flux over the global open oceans for the last two decades. Journal of Oceanography, doi:10.1007/s10872-015-0306-4, 2015.

Ilyina, T., Six, K. D., Segschneider, J., Maier-Reimer, E., Li, H., and Núñez-Riboni, I.: Global ocean biogeochemistry model HAMOCC: Model architecture and performance as component of the MPI-Earth system model in different CMIP5

Field Code Changed

Formatted: No underline

experimental realizations, Journal of Advances in Modeling Earth Systems, 5, 287-315, https://doi.org/10.1029/2012MS000178, 2013.

Jacobson, A. R., Mikaloff Fletcher, S. E., Gruber, N., Sarmiento, J. L., and Gloor, M.: A joint atmosphere-ocean inversion for surface fluxes of carbon dioxide: 1. Methods and global-scale fluxes, Global Biogeochemical Cycles, 21, GB1019, https://doi.org/10.1029/2005GB002556, 2007.

Jacobson, A. R., Schuldt, K. N., Miller, J. B., Oda, T., Tans, P., Andrews, A., Mund, J., Ott, L., Collatz, G. J., Aalto, T., Afshar, S., Aikin, K., Aoki, S., Apadula, F., Baier, B., Bergamaschi, P., Beyersdorf, A., Biraud, S. C., Bollenbacher, A., Bowling, D., Brailsford, G., Abshire, J. B., Chen, G., Chen, H., Chmura, L., Climadat, S., Colomb, A., Conil, S., Cox, A., Cristofanelli, P., Cuevas, E., Curcoll, R., Sloop, C. D., Davis, K., Wekker, S. D., Delmotte, M., DiGangi, J. P., Dlugokencky, E., Ehleringer, J., Elkins, J. W., Emmenegger, L., Fischer, M. L., Forster, G., Frumau, A., Galkowski, M., Gatti, L. V., Gloor, E., Griffis, T., Hammer, S., Haszpra, L., Hatakka, J., Heliasz, M., Hensen, A., Hermanssen, O., Hintsa, E., Holst, J., Jaffe, D., Karion, A., Kawa, S. R., Keeling, R., Keronen, P., Kolari, P., Kominkova, K., Kort, E., Krummel, P., Kubistin, D., Labuschagne, C., Langenfelds, R., Laurent, O., Laurila, T., Lauvaux, T., Law, B., Lee, J., Lehner, I., Leuenberger, M., Levin, I., Levula, J., Lin, J., Lindauer, M., Loh, Z., Lopez, M., Lund Myhre, C., Machida, T., Mammarella, I., Manca, G., Manning, A., Manning, A., Marek, M. V., Marklund, P., Martin, M. Y., Matsueda, H., McKain, K., Meijer, H., Meinhardt, F., Miles, N., Miller, C. E., Mölder, M., Montzka, S., Moore, F., Morgui, J., Morimoto, S., Munger, B., Necki, J., ¨Newman, S., Nichol, S., Niwa, Y., O'Doherty, S., Ottosson-Löfvenius, M., Paplawsky, B., Peischl, J., Peltola, O., Pichon, J., Piper, S., Plass-Dölmer, C., Ramonet, M., Reyes-Sanchez, E., Richardson, S., Riris, H., Ryerson, T., Saito, K., Sargent, M., Sasakawa, M., Sawa, Y., Say, D., Scheeren, B., Schmidt, M., Schmidt, A., Schumacher, M., Shepson, P., Shook, M., Stanley, K., Steinbacher, M., Stephens, B., Sweeney, C., Thoning, K., Torn, M., Turnbull, J., Tørseth, K., van den Bulk, P., van der Laan−Luijkx, I. T., van Dinther, D., Vermeulen, A., Viner, B., Vitkova, G., Walker, S., Weyrauch, D., Wofsy, S., Worthy, D., Young, D., and Zimnoch, M., CarbonTracker CT2019, Model published by NOAA Earth System Research Laboratory, Global Monitoring Division, https://doi.org/ 10.25925/39m3-6069, 2020.

Jones, S. D., Le Quéré, C., and Rödenbeck, C.: Autocorrelation characteristics of surface ocean pCO_2 and air-sea CO_2 fluxes. Global biogeochemical cycles, 26, 2, https://doi.org/10.1029/2010GB004017, 2012

Kang, J. S., Kalnay, E., Liu, J., Fung, I., Miyoshi, T., and Ide, K.: Variable localization" in an ensemble Kalman filter: Application to the carbon cycle data assimilation." Journal of Geophysical Research: Atmospheres, 116, D9 https://doi.org/10.1029/2010JD014673, 2011.

Kang, J. S., Kalnay, E., Miyoshi, T., Liu, J., and Fung, I.: Estimation of surface carbon fluxes with an advanced data assimilation methodology, Journal of Geophysical Research: Atmospheres, 117, D24101, https://doi.org/10.1029/2012JD018259, 2012.

Khatiwala, S. P., Tanhua, T., Mikaloff Fletcher, S. E., Gerber, M., Doney, S. C., Graven, H. D., Gruber, N., McKinley, G., Murata, A., and Ríos, A.: Global ocean storage of anthropogenic carbon, Biogeosciences, 10, 2169-2191, https://doi.org/10.5194/bg-10-2169-2013, 2013.

Formatted: Automatically adjust right indent when grid is defined, Widow/Orphan control, Adjust space between Latin and Asian text, Adjust space between Asian text and numbers, Pattern: Clear (White)

Formatted: Font: (Default) +Body (Times New Roman), Font color: Custom Color(RGB(118,118,118))

Landschützer, P., Gruber, N., Bakker, D. C., Schuster, U., Nakaoka, S. I., Payne, M. R., Sasse, T. P., and Zeng, J.: A neural network-based estimate of the seasonal to inter-annual variability of the Atlantic Ocean carbon sink, Biogeosciences, 10, 7793-7815, https://doi.org/10.5194/bg-10-7793-2013, 2013.

Landschuetzer, P., Gruber, N., and Bakker, D. C.: Decadal variations and trends of the global ocean carbon sink, Global Biogeochemical Cycles, 30, 1396-1417, https://doi.org/10.1002/2015GB005359, 2016.

~~Landschützer, P., Gruber, N., Bakker, D. C., Schuster, U., Nakaoka, S. I., Payne, M. R., Sasse, T. P., and Zeng, J.: A neural network-based estimate of the seasonal to inter-annual variability of the Atlantic Ocean carbon sink, Biogeosciences, 10, 7793-7815, https://doi.org/10.5194/bg-10-7793-2013, 2013.~~

Landschützer, P., Ilyina, T., and Lovenduski, N. S.: Detecting Regional Modes of Variability in Observation-Based Surface Ocean pCO_2, Geophysical Research Letters, 46, 2670-2679, https://doi.org/10.1029/2018GL081756, 2019.

Law, R. M., Ziehn, T., Matear, R. J., Lenton, A., Chamberlain, M. A., Stevens, L. E., Ying-Ping, W., Srbinovsky, J., Bi, D., and Yan, H.: The carbon cycle in the Australian Community Climate and Earth System Simulator (ACCESS-ESM1)–Part 1: Model description and pre-industrial simulation, Geoscientific Model Development, 10, 2567-2590, https://doi.org/10.6194/gmd-10-2567-2017, 2017.

Le Quéré, C., Andrew, R. M., Friedlingstein, P., Sitch, S., Pongratz, J., Manning, A. C., Korsbakken, J. I., Peters, G. P., Canadell, J. G., Jackson, R. B., Boden, T. A., Tans, P. P., Andrews, O. D., Arora, V. K., Bakker, D. C. E., Barbero, L., Becker, M., Betts, R. A., Bopp, L., Chevallier, F., Chini, L. P., Ciais, P., Cosca, C. E., Cross, J., Currie, K., Gasser, T., Harris, I., Hauck, J., Haverd, V., Houghton, R. A., Hunt, C. W., Hurtt, G., Ilyina, T., Jain, A. K., Kato, E., Kautz, M., Keeling, R. F., Klein Goldewijk, K., Körtzinger, A., Landschützer, P., Lefèvre, N., Lenton, A., Lienert, S., Lima, I., Lombardozzi, D., Metzl, N., Millero, F., Monteiro, P. M. S., Munro, D. R., Nabel, J. E. M. S., Nakaoka, S., Nojiri, Y., Padin, X. A., Peregon, A., Pfeil, B., Pierrot, D., Poulter, B., Rehder, G., Reimer, J., Rödenbeck, C., Schwinger, J., Séférian, R., Skjelvan, I., Stocker, B. D., Tian, H., Tilbrook, B., Tubiello, F. N., van der Laan−Luijkx, I. T., van der Werf, G. R., van Heuven, S., Viovy, N., Vuichard, N., Walker, A. P., Watson, A. J., Wiltshire, A. J., Zaehle, S., and Zhu, D.: Global carbon budget 2017, Earth System Science Data, 10, 405-448, https://doi.org/10.5194/essd-10-405-2018, 2018.

Lebehot, A. D., Halloran, P. R., Watson, A. J., McNeall, D., Ford, D. A., Landschützer, P., Lauvset, S. K., and Schuster, U.: Reconciling observation and model trends in North Atlantic surface CO_2, Global Biogeochemical Cycles, 33, 1204-1222, https://doi.org/10.1029/2019GB006186, 2019.

~~Liu, J., Bowman, K. W., and Henze, D. K.: Source-receptor relationships of column-average CO_2 and implications for the impact of observations on flux inversions, Journal of Geophysical Research: Atmospheres, 120, 5214-5236, https://doi.org/10.1002/2014JD022914, 2015.~~

Liu, J., Bowman, K. W., and Lee, M.: Comparison between the Local Ensemble Transform Kalman Filter (LETKF) and 4D-Var in atmospheric CO_2 flux inversion with the Goddard Earth Observing System-Chem model and the observation impact diagnostics from the LETKF, Journal of Geophysical Research: Atmospheres, 121, 13,066-013,087,

https://doi.org/10.1002/2016JD025100, 2016.

Liu, Y., Kalnay, E., Zeng, N., Asrar, G., Chen, Z., and Jia, B.: Estimating surface carbon fluxes based on a local ensemble transform Kalman filter with a short assimilation window and a long observation window: an observing system simulation experiment test in GEOS-Chem 10.1, Geoscientific Model Development, 12, 2899-2914, https://doi.org/10.5194/gmd-12-2899-2019, 2019.

Macovei, V. A., Hartman, S. E., Schuster, U., Torres-Valdés, S., Moore, C. M., and Sanders, R. J.: Impact of physical and biological processes on temporal variations of the ocean carbon sink in the mid-latitude North Atlantic (2002–2016), Progress in Oceanography, 180, 102223, https://doi.org/10.1016/j.pocean.2019.102223, 2020.

McKinley, G. A., Fay, A. R., Takahashi, T., and Metzl, N.: Convergence of atmospheric and North Atlantic carbon dioxide trends on multidecadal timescales, Nature Geoscience, 4, 606-610, https://doi.org/10.1038/ngeo1193, 2011.

Mikaloff Fletcher, S., Gruber, N., Jacobson, A. R., Doney, S., Dutkiewicz, S., Gerber, M., Follows, M., Joos, F., Lindsay, K., and Menemenlis, D.: Inverse estimates of anthropogenic CO_2 uptake, transport, and storage by the ocean, Global Biogeochemical Cycles, 20, GB2002, https://doi.org/10.1029/2005GB002530, 2006.

Miyoshi, T., Yamane, S., and Enomoto, T.: Localizing the error covariance by physical distances within a local ensemble transform Kalman filter (LETKF), SOLA, 3, 089-092, https://doi.org/10.2151/sola.2007-023, 2007.

Montgomery, D. C., Peck, E. A., and Vining, G. G.: Introduction to Linear Regression Analysis,5th Edition, John Wiley & Sons, 2012.

Nassar, R., Jones, D. B., Suntharalingam, P., Chen, J. M., Andres, R. J., Wecht, K. J., Yantosca, R. M., Kulawik, S. S., Bowman, K. W., and Worden, J. R.: Modeling global atmospheric CO_2 with improved emission inventories and CO_2 production from the oxidation of other carbon species, Geoscientific Model Development, 3, 689-716, https://doi.org/10.5194/gmd-3-689-2010, 2010.

Nassar, R., Jones, D. B. A., Kulawik, S. S., Worden, J. R., Bowman, K. W., Andres, R. J., Suntharalingam, P., Chen, J. M., Brenninkmeijer, C., and Schuck, T.: Inverse modeling of CO_2 sources and sinks using satellite observations of CO_2 from TES and surface flask measurements, Atmospheric Chemistry and Physics, 11, 6029-6047, https://doi.org/10.5194/acp-11-6029-2011, 2011.

Peters, W., Miller, J., Whitaker, J., Denning, A., Hirsch, A., Krol, M., Zupanski, D., Bruhwiler, L., and Tans, P.: An ensemble data assimilation system to estimate CO_2 surface fluxes from atmospheric trace gas observations, Journal of Geophysical Research: Atmospheres, 110, D24304, https://doi.org/10.1029/2005JD006157, 2005.

Peylin, P., Law, R., Gurney, K., Chevallier, F., Jacobson, A., Maki, T., Niwa, Y., Patra, P., Peters, W., and Rayner, P.: Global atmospheric carbon budget: results from an ensemble of atmospheric CO_2 inversions, Biogeosciences, 10, 6699-6720, https://doi.org/10.5194/bg-10-6699-2013, 2013.

Rienecker, M. M., Suarez, M., Todling, R., Bacmeister, J., Takacs, L., Liu, H., Gu, W., Sienkiewicz, M., Koster, R., and Gelaro, R.: The GEOS-5 Data Assimilation System: Documentation of Versions 5.0. 1, 5.1. 0, and 5.2. 0, NASA Technical Report Series on Global Modelling and Data Assimilation,NASA/TM–2008–104606, 27, 2008.

Rödenbeck, C., Houweling, S., Gloor, M., and Heimann, M.: Time-dependent atmospheric CO_2 inversions based on interannually varying tracer transport, Tellus, 55B, 488-497, https://doi.org/10.3402/tellusb.v55i2.16707, 2003.

Rödenbeck, C., Keeling, R. F., Bakker, D. C., Metzl, N., Olsen, A., Sabine, C., and Heimann, M.: Global surface-ocean pCO_2 and sea–air CO_2 flux variability from an observation-driven ocean mixed-layer scheme. Ocean Science, 9, 2, 193-216, https://doi.org/10.5194/os-9-193-2013, 2013.

Rödenbeck , C., Bakker, D. C. E., Metzl, N., Olsen, A., Sabine, C., Reum, F., Keeling, R. F., and Heimann, M.: Interannual sea-air CO_2 flux variability from an observation-driven ocean mixed-layer scheme, Biogeosciences, 11, 4599-4613, https://doi.org/10.5194/bg-11-4599-2014, 2014.

Rödenbeck, C., Bakker, D. C., Gruber, N., Iida, Y., Jacobson, A. R., Jones, S., Landschützer, P., Metzl, N., Nakaoka, S., and Olsen, A.: Data-based estimates of the ocean carbon sink variability–first results of the Surface Ocean pCO_2 Mapping intercomparison (SOCOM), Biogeosciences, 12, 7251-7278, https://doi.org/10.5194/bg-12-7251-2015, 2015.

Sabine, C. L., Feely, R. A., Gruber, N., Key, R. M., Lee, K., Bullister, J. L., Wanninkhof, R., Wong, C., Wallace, D. W., and Tilbrook, B.: The oceanic sink for anthropogenic CO_2, Science, 305, 367-371, https://doi.org/10.1126/science.1097403, 2004.

Schuster, U., McKinley, G. A., Bates, N., Chevallier, F., Doney, S. C., Fay, A., González-Dávila, M., Gruber, N., Jones, S., and Krijnen, J.: An assessment of the Atlantic and Arctic sea-air CO_2 fluxes, 1990-2009, Biogeosciences, 10, 607-627, https://doi.org/10.5194/bg-10-607-2013, 2013.

Schwinger, J., Goris, N., Tjiputra, J. F., Kriest, I., Bentsen, M., Bethke, I., Ilicak, M., Assmann, K. M., and Heinze, C.: Evaluation of NorESM-OC (versions 1 and 1.2), the ocean carbon-cycle stand-alone configuration of the Norwegian Earth System Model (NorESM1), Geoscientific Model Development, 9, 2589-2622, https://doi.org/10.5194/gmd-9-2589-2016, 2016.

Séférian, R., Bopp, L., Gehlen, M., Orr, J. C., Ethé, C., Cadule, P., Aumont, O., y Mélia, D. S., Voldoire, A., and Madec, G.: Skill assessment of three earth system models with common marine biogeochemistry, Climate Dynamics, 40, 2549-2573, https://doi.org/10.1007/s00382-012-1362-8, 2013.

Suntharalingam, P., Randerson, J. T., Krakauer, N., Logan, J. A., and Jacob, D. J.: Influence of reduced carbon emissions and oxidation on the distribution of atmospheric CO_2: Implications for inversion analyses, Global Biogeochemical Cycles, 19, GB4003, https://doi.org/10.1029/2005GB002466, 2005.

~~Séférian, R., Bopp, L., Gehlen, M., Orr, J. C., Ethé, C., Cadule, P., Aumont, O., y Mélia, D. S., Voldoire, A., and Madec, G.: Skill assessment of three earth system models with common marine biogeochemistry, Climate Dynamics, 40, 2549-2573, https://doi.org/10.1007/s00382-012-1362-8, 2013.~~

Takahashi, T., Sutherland, S. C., Sweeney, C., Poisson, A., Metzl, N., Tilbrook, B., Bates, N., Wanninkhof, R., Feely, R. A., and Sabine, C.: Global sea–air CO_2 flux based on climatological surface ocean pCO_2, and seasonal biological and temperature effects, Deep Sea Research Part II: Topical Studies in Oceanography, 49, 1601-1622, https://doi.org/10.1016/S0967-0645(02)00003-6, 2002.

Formatted: Font: (Default) +Body (Times New Roman)

Takahashi, T., Sutherland, S. C., Wanninkhof, R., Sweeney, C., Feely, R. A., Chipman, D. W., Hales, B., Friederich, G., Chavez, F., and Sabine, C.: Climatological mean and decadal change in surface ocean pCO_2, and net sea–air CO_2 flux over the global oceans, Deep Sea Research Part II: Topical Studies in Oceanography, 56, 554-577, https://doi.org/10.1016/j.dsr2.2008.12.009, 2009.

Van Der Laan−Luijkx, I. T., Van Der Velde, I. R., Van Der Veen, E., Tsuruta, A., Stanislawska, K., Babenhauserheide, A., Zhang, H. F., Liu, Y.-N., He, W., and Chen, H.: The CarbonTracker Data Assimilation Shell (CTDAS) v1. 0: implementation and global carbon balance 2001-2015, Geoscientific Model Development, 10, 2785-2800, https://doi.org/10.5194/gmd-10-2785-2017, 2017.

Wanninkhof, R., Pickers, P., Omar, A., Sutton, A., Murata, A., Olsen, A., Bb, S., Tilbrook, B., Munro, D., and Pierrot, D.: A surface ocean CO_2 reference network, SOCONET and associated marine boundary layer CO_2 measurements, Frontiers in Marine Science, 6, https://doi.org/10.3389/fmars.2019.00400, 2019.

Watson, A. J., Schuster, U., Bakker, D. C., Bates, N. R., Corbière, A., González-Dávila, M., Friedrich, T., Hauck, J., Heinze, C., and Johannessen, T.: Tracking the variable North Atlantic sink for atmospheric CO_2, Science, 326, 1391-1393, https://doi.org/10.1126/science.1177394, 2009.

Watson, A. J., Schuster, U., Shutler, J. D., Holding, T., Ashton, I. G. C., Landschützer, P., Woolf, D. K., and Goddijn-Murphy, L.: Revised estimates of ocean-atmosphere CO2 flux are consistent with ocean carbon inventory, Nat. Commun., 11, 1–6, https://doi.org/10.1038/s41467-020-18203-3, 2020.

Zeng, J., Nojiri, Y., Nakaoka, Shin-ichiro, Nakajima, H. and Shirai, T.: Surface ocean CO_2 in 1990–2011 modelled using a feed-forward neural network. Geoscience Data Journal, 2: 47-51. https://doi.org/10.1002/gdj3.26, 2015.